# A nonclassical vitamin D receptor pathway suppresses renal fibrosis

Ichiaki Ito,[1] Tsuyoshi Waku,[2] Masato Aoki,[1] Rumi Abe,[3] Yu Nagai,[3] Tatsuya Watanabe,[1] Yuka Nakajima,[1] Ichiro Ohkido,[4] Keitaro Yokoyama,[4] Hiroyuki Miyachi,[5] Toshiyuki Shimizu,[2] Akiko Murayama,[1] Hiroyuki Kishimoto,[1] Kazuo Nagasawa,[3] and Junn Yanagisawa[1]

[1]Graduate School of Life and Environmental Sciences/Life Science Center of Tsukuba Advanced Research Alliance, University of Tsukuba, Tsukuba Science City, Ibaraki, Japan. [2]Graduate School of Pharmaceutical Sciences, The University of Tokyo, Bunkyo-ku, Tokyo, Japan. [3]Department of Biotechnology and Life Science, Faculty of Technology, Tokyo University of Agriculture and Technology, Koganei, Tokyo, Japan. [4]Division of Nephrology and Hypertension, Department of Internal Medicine, Jikei University School of Medicine, Minato-ku, Tokyo, Japan. [5]Graduate School of Medicine, Dentistry and Pharmaceutical Sciences, Okayama University, Kita-ku, Okayama, Japan.

**The TGF-β superfamily comprises pleiotropic cytokines that regulate SMAD and non-SMAD signaling. TGF-β–SMAD signal transduction is known to be involved in tissue fibrosis, including renal fibrosis. Here, we found that 1,25-dihydroxyvitamin $D_3$–bound [1,25$(OH)_2D_3$-bound] vitamin D receptor (VDR) specifically inhibits TGF-β–SMAD signal transduction through direct interaction with SMAD3. In mouse models of tissue fibrosis, 1,25$(OH)_2D_3$ treatment prevented renal fibrosis through the suppression of TGF-β–SMAD signal transduction. Based on the structure of the VDR-ligand complex, we generated 2 synthetic ligands. These ligands selectively inhibited TGF-β–SMAD signal transduction without activating VDR-mediated transcription and significantly attenuated renal fibrosis in mice. These results indicate that 1,25$(OH)_2D_3$-dependent suppression of TGF-β–SMAD signal transduction is independent of VDR-mediated transcriptional activity. In addition, these ligands did not cause hypercalcemia resulting from stimulation of the transcriptional activity of the VDR. Thus, our study provides a new strategy for generating chemical compounds that specifically inhibit TGF-β–SMAD signal transduction. Since TGF-β–SMAD signal transduction is reportedly involved in several disorders, our results will aid in the development of new drugs that do not cause detectable adverse effects, such as hypercalcemia.**

## Introduction

The TGF-β superfamily is a large, evolutionarily conserved group of cytokines (1, 2). TGF-β regulates a wide range of cellular processes by signaling through high-affinity TGF-β receptors (3–6). Binding of TGF-β to its receptors triggers phosphorylation of SMAD transcription factors, which are central mediators of TGF-β signal transduction (7–9). SMAD2 and SMAD3 are receptor activated, whereas SMAD4 serves as a common partner for all receptor-activated SMAD proteins (10–12). Signaling pathways involving non-SMAD proteins such as MAPK or PI3K are activated directly by ligand-bound TGF-β receptors to reinforce, attenuate, or otherwise modulate downstream cellular responses (13).

Perturbations in TGF-β signal transduction play a role in numerous human diseases. For instance, upregulated TGF-β production has been linked to fibrotic disease (14–17) and cancer progression (18, 19). Furthermore, activation of SMAD signaling by TGF-β exacerbates tissue fibrosis (15, 20–23). Numerous studies show that SMAD3 deficiency in mice attenuated cutaneous (24), hepatic (25), renal (26–28), and pulmonary (29) fibrosis. Although TGF-β and TGF-β receptor blockers have been developed for clinical use, current understanding of the pathologic roles of SMAD proteins suggest that specifically targeting SMAD signaling may result in better therapeutic profiles.

The vitamin D receptor (VDR) is a member of the nuclear receptor superfamily and functions as a ligand-inducible transcription factor (30–32). Binding of 1,25-dihydroxyvitamin $D_3$ [1,25$(OH)_2D_3$] to the receptor ligand-binding domain (LBD) of the VDR induces a conformational change in the receptor and dimerization with retinoid X receptors. The resulting heterodimers then bind DNA, vitamin D–responsive element (VDRE), to stimulate gene expression (classical genomic action). The VDR-LBD is crucial for ligand-dependent transcriptional activity (33). Crystal structure analyses indicate that the LBDs of the VDR and other nuclear receptors contain 12 conserved helices (34). Of particular note, the C-terminal helix 12 (H12) in LBD plays an important role in binding coactivators, including SRC-1, to the ligand-bound receptor (35). VDR modulates the transcription of vitamin D–regulated genes involved in intestinal calcium/phosphate absorption and remodeling of bone to maintain calcium homeostasis. Although direct regulation of gene expression by VDR depends on the presence of VDRE in the promoters of target genes, some 1,25$(OH)_2D_3$-regulated genes do not contain VDRE in their promoters and are thought to be regulated indirectly. Thus, VDR can not only affect gene expression by binding to VDRE, but can also regulate other gene expressions by associating with several transcription factors, such as Sp1 (36) and β-catenin/TCF (37, 38). In addition to the classical genomic action, 1,25$(OH)_2D_3$ has also been shown to initiate many biological responses via the rapid response pathway of VDR. The localization of VDR to the plasma membrane caveolae results in activation of signal transduction pathways that generate rapid responses, such as transcaltachia or insulin secretion, which are activated by signal via plasma membrane–localized VDR (nongenomic action) (39).

Deficiencies in vitamin D and its active metabolites are known pathologic features of chronic kidney diseases (40). Previous studies have shown that vitamin D supplementation suppresses renal fibrosis (41–48). These studies have suggested that vitamin D

**Conflict of interest:** The authors have declared that no conflict of interest exists.
**Citation for this article:** *J Clin Invest.* 2013;123(11):4579–4594. doi:10.1172/JCI67804.

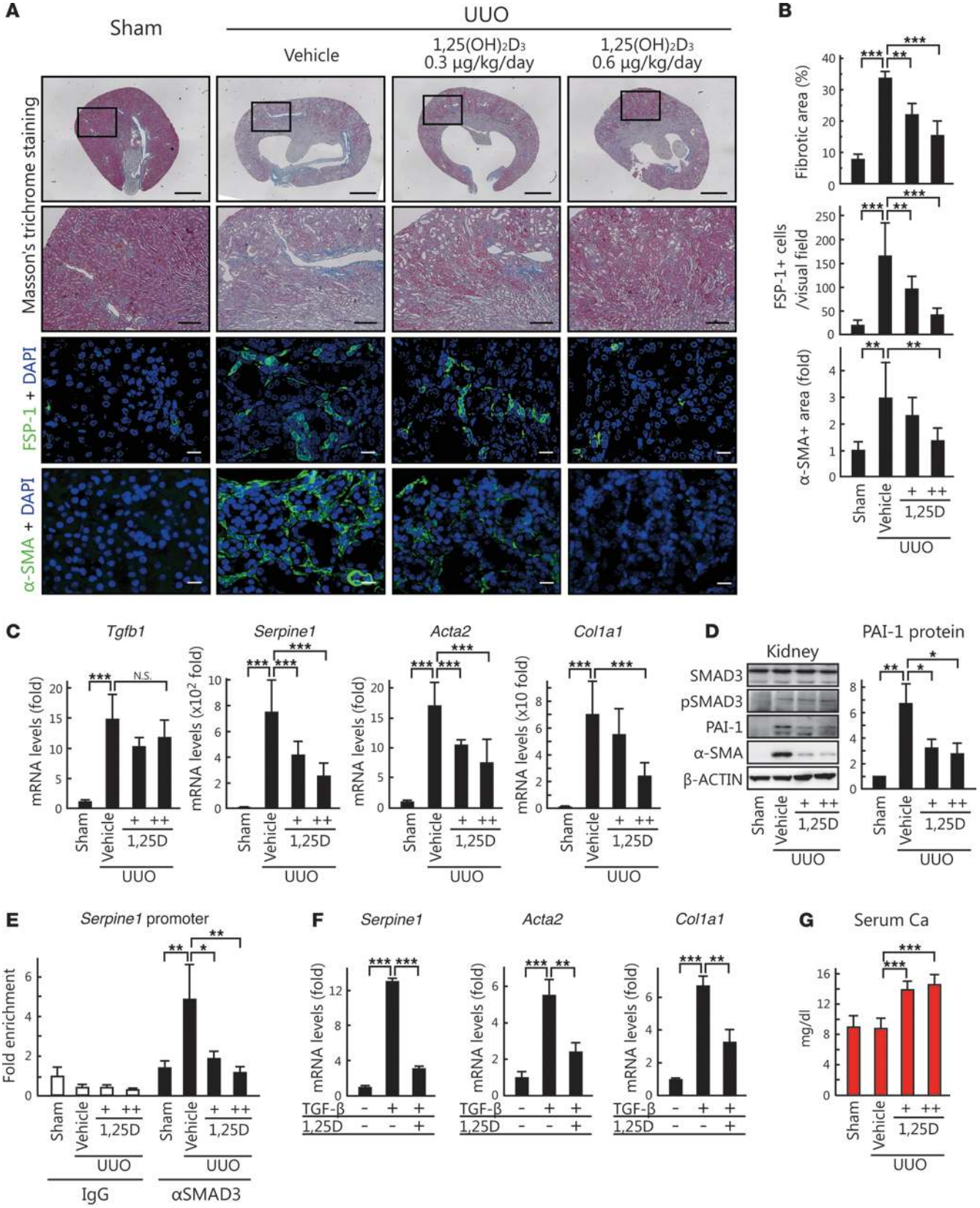
A
Sham
UUO
Vehicle
1,25(OH)2D3 0.3 μg/kg/day
1,25(OH)2D3 0.6 μg/kg/day
Masson's trichrome staining
FSP-1 + DAPI
α-SMA + DAPI
B
Fibrotic area (%)
FSP-1+ cells /visual field
α-SMA+ area (fold)
Sham
Vehicle
+
++
1,25D
UUO
C
Tgfb1
Serpine1
Acta2
Col1a1
mRNA levels (fold)
mRNA levels (x10² fold)
mRNA levels (x10 fold)
N.S.
D
Kidney
SMAD3
pSMAD3
PAI-1
α-SMA
β-ACTIN
PAI-1 protein
E
Serpine1 promoter
Fold enrichment
IgG
αSMAD3
F
Serpine1
Acta2
Col1a1
TGF-β
1,25D
G
Serum Ca
mg/dl

**Figure 1**
$1,25(OH)_2D_3$ suppresses renal fibrosis by inhibiting TGF-β signal transduction in UUO mice. (**A**) Representative photomicrographs of Masson's trichrome staining (top row, whole kidney; second row, magnified view of boxed region, enlarged ×4.37), FSP-1– (third row), or α-SMA–specific immunofluorescence staining (bottom row) of kidney sections from sham-operated control or UUO mice injected with vehicle or $1,25(OH)_2D_3$. Scale bars: 1.0 mm (top row); 200 μm (second row); 20 μm (bottom 2 rows). (**B**) Fibrotic areas ($n$ = 4 per group), FSP-1–positive cells ($n$ = 12 per group), and α-SMA–positive areas ($n$ = 8 per group) in stained sections were quantified. 1,25D, $1,25(OH)_2D_3$; +, 0.3 μg/kg/d; ++, 0.6 μg/kg/d. (**C**) RNA was isolated from the kidneys of mice treated with vehicle ($n$ = 16) or $1,25(OH)_2D_3$ (0.3 or 0.6 μg/kg/d) after being subjected to UUO ($n$ = 10 or 6, respectively) or sham operation ($n$ = 6). *Tgfb1*, *Serpine1*, *Acta2*, and *Col1a1* mRNA expression was determined using qPCR. (**D**) Western blotting analysis of kidney protein levels. Quantification of PAI-1 protein levels in each treatment group ($n$ = 3 per group) is shown at right. (**E**) Kidney samples were subjected to ChIP assay using control IgG or anti-SMAD3 antibodies. (**F**) Kidney fibroblasts were cultured in the presence or absence of TGF-β (5 ng/ml) and $1,25(OH)_2D_3$ (10 nM) for 8 hours, after which *Serpine1*, *Acta2*, and *Col1a1* mRNA levels were determined by qPCR. (**G**) Serum calcium concentration. $^*P < 0.05$; $^{**}P < 0.01$; $^{***}P < 0.001$.

metabolites and its synthetic analogs may play a role in therapeutic suppression of renal fibrosis through stimulation of VDR-mediated transcription, although there is little agreement concerning the underlying mechanism.

Here, we report that the VDR inhibits TGF-β–SMAD signal transduction. Our results indicate that the VDR decreases TGF-β–dependent SMAD transcriptional activity by inhibiting recruitment of SMAD3 to the promoter regions of TGF-β target genes in a $1,25(OH)_2D_3$-dependent manner. Animal model experiments revealed that $1,25(OH)_2D_3$ suppressed renal fibrosis by inhibiting TGF-β–SMAD signal transduction. Using computational structural analysis, we identified 2 synthetic VDR ligands — the 1α,25-dihydroxyvitamin $D_3$-26,23-lactam (DLAM) derivatives DLAM-iPr and DLAM-4P — that selectively inhibited TGF-β–SMAD signal transduction without activation of classical VDR-mediated transcription. The effective dose of $1,25(OH)_2D_3$ cannot be used clinically because it results in significant hypercalcemia. In contrast, DLAM-iPr and DLAM-4P suppressed renal fibrosis in a mouse model without causing hypercalcemia. Thus, inhibition of TGF-β–SMAD signal transduction through VDR nonclassical pathway suppresses renal fibrosis. Our findings provide new insights relevant to the functions of the VDR and to the development of drugs to treat TGF-β–related diseases.

## Results

*VDR suppresses renal fibrosis in mice subjected to unilateral ureteral obstruction via inhibition of TGF-β–SMAD signal transduction.* It has been reported that the VDR plays a role in therapeutic suppression of renal fibrosis (41–49), although there is little agreement concerning the underlying mechanism. Previous studies have suggested that activation of SMAD signaling by TGF-β exacerbates tissue fibrosis (15, 20–23). Therefore, we examined whether $1,25(OH)_2D_3$ suppresses renal fibrosis by inhibiting TGF-β–SMAD signal transduction in mice subjected to unilateral ureteral obstruction (UUO), an established model of tubulointerstitial renal fibrosis. Masson's trichrome staining of renal tissues in mice revealed that aniline blue–positive areas in UUO kidneys were significantly larger than those in sham-operated control kidneys (Figure 1, A and B). In contrast, stained areas were significantly smaller in the kidneys of $1,25(OH)_2D_3$-treated versus untreated UUO mice. Staining using fibroblast-specific protein–1 (FSP-1) and α-SMA as markers of renal fibrosis revealed the progression of fibrosis in the kidneys of UUO mice, whereas administration of $1,25(OH)_2D_3$ produced dose-dependent decreases in FSP-1– and α-SMA–positive cells (Figure 1, A and B).

UUO kidneys contained 15-fold more *Tgfb1* mRNA than did control kidneys (Figure 1C). Western blot analysis revealed that the level of phosphorylated SMAD3 (pSMAD3) was higher in UUO kidneys (Figure 1D and Supplemental Figure 1A; supplemental material available online with this article; doi:10.1172/JCI67804DS1), indicative of activation of TGF-β–SMAD signal transduction. We then examined the expression of 3 TGF-β target genes involved in fibrosis: *Serpine1* (encoding plasminogen activator inhibitor 1 [PAI-1]), *Acta2* (encoding α-SMA), and *Col1a1* (encoding type I collagen) (50). Real-time quantitative RT-PCR (qPCR) analysis showed that *Serpine1*, *Acta2*, and *Col1a1* mRNA levels increased in UUO versus control kidneys (Figure 1C). Interestingly, $1,25(OH)_2D_3$ treatment did not affect the levels of *Tgfb* mRNA and pSMAD3 in UUO kidneys, whereas *Serpine1*, *Acta2*, and *Col1a1* expression was dose-dependently decreased by $1,25(OH)_2D_3$ (Figure 1, C and D, and Supplemental Figure 1A). In addition, ChIP assay revealed an increased level of SMAD3 binding to the *Serpine1* promoter in UUO kidneys, which was decreased by $1,25(OH)_2D_3$ treatment (Figure 1E).

Based on these data, it is reasonable to suggest that $1,25(OH)_2D_3$ suppresses TGF-β–SMAD signal transduction in UUO kidneys. To test this possibility, we isolated mouse kidney fibroblasts (Supplemental Figure 2) and examined the effects of $1,25(OH)_2D_3$ on expression of TGF-β target genes. As expected, TGF-β stimulated *Serpine1*, *Acta2*, and *Col1a1* mRNA expression, which was decreased by $1,25(OH)_2D_3$ treatment (Figure 1F). These results suggest that $1,25(OH)_2D_3$ ameliorates TGF-β–SMAD signal transduction, which may lead to suppression of renal fibrosis.

Meanwhile, $1,25(OH)_2D_3$ also significantly increased the serum calcium level (Figure 1G), which reflects a dysregulation of calcium homeostasis resulting from stimulation of the transcriptional activity of the VDR. Thus, although $1,25(OH)_2D_3$ may be therapeutic for renal fibrosis, the associated elevation in serum calcium may have serious adverse consequences that would prevent its clinical application.

*$1,25(OH)_2D_3$ inhibits recruitment of SMAD3 to TGF-β target gene promoters.* We next examined the effects of $1,25(OH)_2D_3$ on expression of TGF-β target genes in the murine renal epithelial TCMK-1 cell line. qPCR analysis confirmed that $1,25(OH)_2D_3$ induced expression of the VDR target gene *Cyp24a1* (Figure 2A). Treatment of TCMK-1 cells with TGF-β increased *Serpine1* and *Acta2* transcription (Figure 2A). The TGF-β–dependent elevation of *Serpine1* mRNA was reduced in a $1,25(OH)_2D_3$-dependent manner (Figure 2A). Knocking down VDR expression in TCMK-1 cells abolished the effect of $1,25(OH)_2D_3$ on *Serpine1* expression (Figure 2B and Supplemental Figure 1B). TGF-β–dependent elevation of *Acta2* mRNA levels was also reduced in a $1,25(OH)_2D_3$-dependent manner (Figure 2A).

To explore the mechanism underlying VDR-dependent inhibition of TGF-β–SMAD signal transduction, we evaluated the effect of $1,25(OH)_2D_3$ on phosphorylation levels and nuclear transloca-

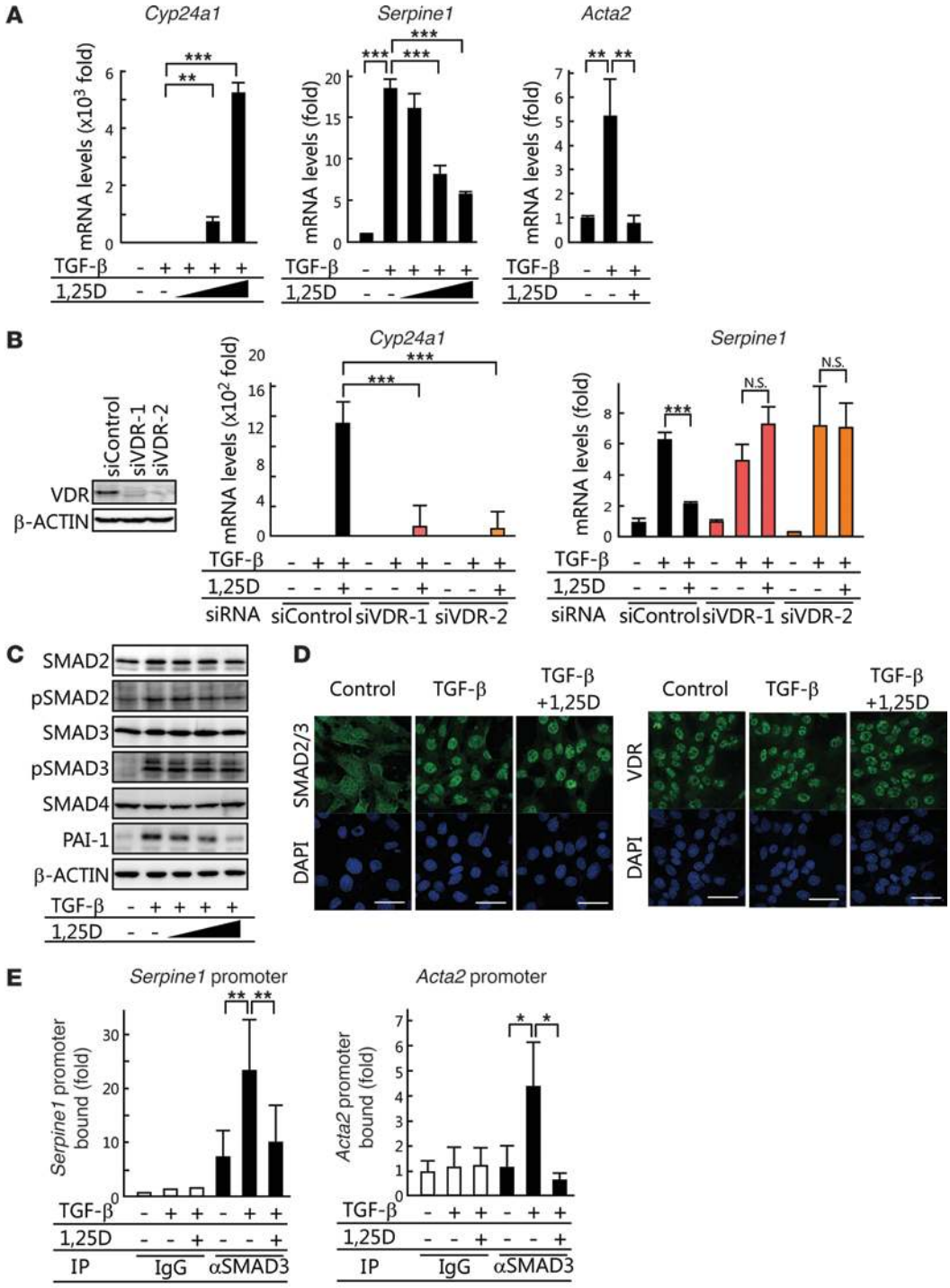


**Figure 2**

$1,25(OH)_2D_3$ inhibits TGF-β–dependent transcription via VDR. (**A**) TCMK-1 cells were cultured in the presence or absence of 5 ng/ml TGF-β and 0.001, 0.1, or 10 nM (+) $1,25(OH)_2D_3$ for 8 hours, and *Cyp24a1*, *Serpine1*, and *Acta2* mRNA levels were determined using qPCR. (**B**) Knockdown of VDR expression eliminated the effects of $1,25(OH)_2D_3$ on TGF-β–induced *Serpine1* expression in TCMK-1 cells. Western blotting confirmed reduced expression of VDR protein in response to 2 VDR-specific siRNAs (siVDR-1 and siVDR-2). *Cyp24a1* and *Serpine1* mRNA levels in response to VDR knockdown and treatment with 5 ng/ml TGF-β and/or 10 nM $1,25(OH)_2D_3$ were determined. (**C**) TCMK-1 cells were treated with or without 5 ng/ml TGF-β and 0.001, 0.1, or 10 nM $1,25(OH)_2D_3$. SMAD2, pSMAD2, SMAD3, pSMAD3, SMAD4, PAI-1, and β-actin protein levels were determined by Western blotting. (**D**) TCMK-1 cells cultured in the presence or absence of 5 ng/ml TGF-β or 10 nM $1,25(OH)_2D_3$ were stained with anti-SMAD2/3 or anti-VDR antibodies. Scale bars: 50 μm. (**E**) ChIP assay was performed with control IgG or anti-SMAD3 antibodies. Immunoprecipitated DNA was examined using qPCR with primers specific for the *Serpine1* or *Acta2* promoter. $^*P < 0.05$; $^{**}P < 0.01$; $^{***}P < 0.001$.

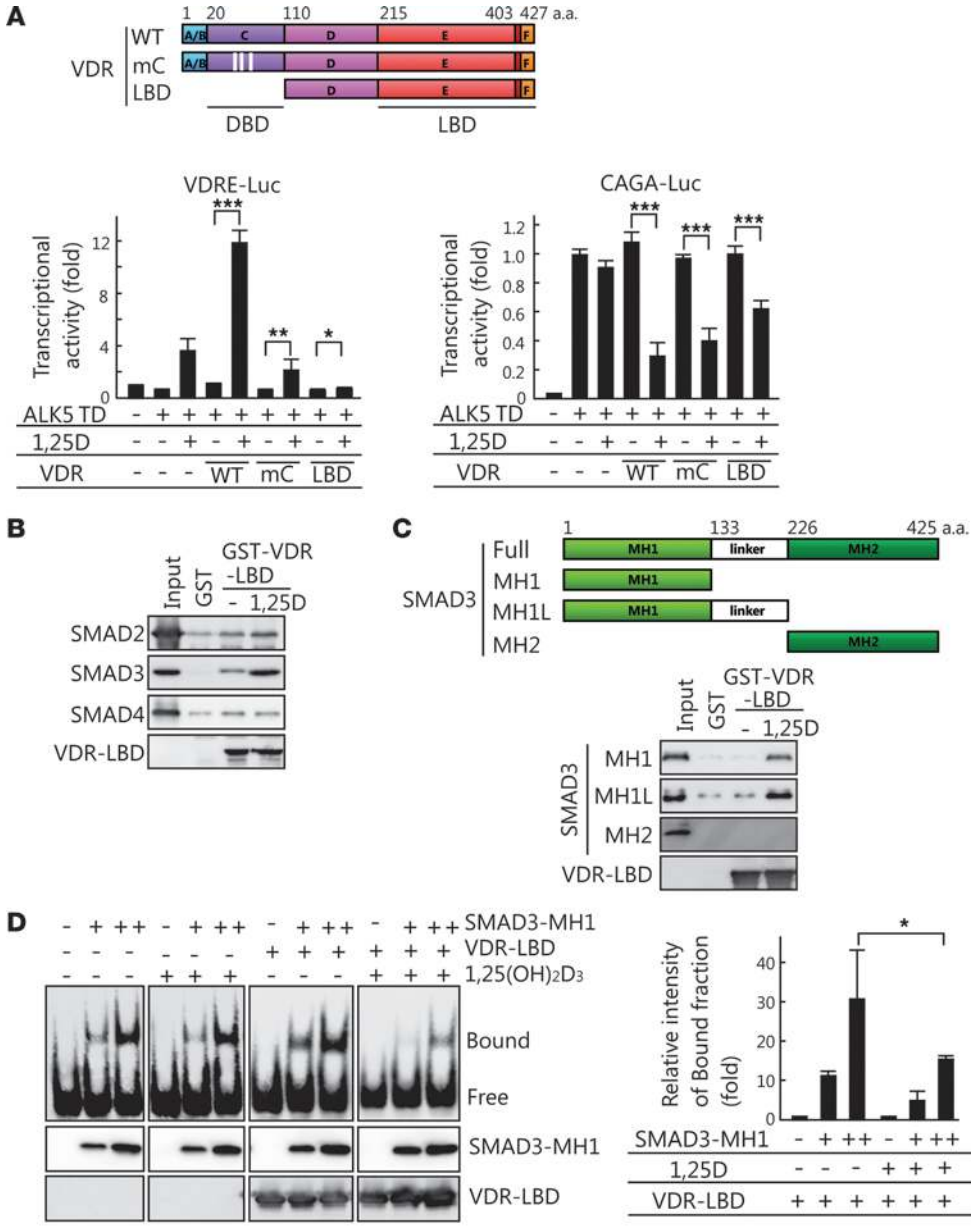


**Figure 3**

$1,25(OH)_2D_3$ disrupts binding of SMAD3 to DNA via VDR. (**A**) VDR mutants lacking DNA binding activity due to mutation or deletion of the C domain are shown at top. HEK293 cells were transfected with plasmids encoding ALK5 TD, VDR, VDR-mC, or VDR-LBD and the reporter plasmids VDRE-Luc or CAGA-Luc. After culturing transfected cells with or without $1,25(OH)_2D_3$ for 24 hours, cell extracts were analyzed using luciferase assay. DBD, DNA-binding domain. (**B**) Purified recombinant His-tagged SMAD2, SMAD3, and SMAD4 were incubated with GST-VDR-LBD in the presence or absence of $1,25(OH)_2D_3$. (**C**) Purified recombinant His-tagged SMAD3-MH1 (aa 1–132), SMAD3-MH1L (aa 1–225), or SMAD3-MH2 (aa 226–425) were incubated with GST-VDR-LBD in the presence or absence of $1,25(OH)_2D_3$, after which the mixtures were examined using in vitro pulldown assay. (**D**) Recombinant SMAD3-MH1 and/or VDR-LBD were mixed with a DNA probe containing the SMAD3-binding element in the presence or absence of $1,25(OH)_2D_3$, after which binding between SMAD3-MH1 and the probe was analyzed by EMSA. Protein levels were determined by Western blotting. The quantified shifted band (bound fraction) is shown at right ($n$ = 3). + and ++ indicate the ratios of sample volumes applied to the assay. $^*P < 0.05$; $^{**}P < 0.01$; $^{***}P < 0.001$.

tion of SMAD2 and SMAD3. Western blot analysis revealed that TGF-β–induced pSMAD2 and pSMAD3 levels were not affected by $1,25(OH)_2D_3$ (Figure 2C and Supplemental Figure 1C). In addition, PAI-1 and α-SMA levels were decreased (Figure 2C and Supplemental Figure 1C). Immunofluorescence staining revealed that TGF-β–induced nuclear accumulation of SMAD2 and SMAD3 was not affected by $1,25(OH)_2D_3$ (Figure 2D). We next examined the recruitment of SMAD3 to the *Serpine1* and *Acta2* promoter regions, since SMAD3 has DNA-binding ability (51). ChIP assay demonstrated that the interaction between SMAD3 and the *Serpine1* or *Acta2* promoter was potentiated by TGF-β, but was suppressed in the presence of $1,25(OH)_2D_3$ (Figure 2E). In addition, $1,25(OH)_2D_3$-dependent suppression of *Serpine1* expression and inhibition of SMAD3 binding to the *Acta2* promoter were also observed in the human renal proximal tubular epithelial HK-2 cell line (Supplemental Figure 3). These results suggest that VDR suppresses TGF-β–SMAD signal transduction by reducing the recruitment of SMAD3 to TGF-β target genes in an $1,25(OH)_2D_3$-dependent manner.

To determine the role of VDR in inhibiting SMAD3 recruitment to TGF-β target genes, we sought to identify the VDR regions responsible for inhibiting TGF-β–SMAD signal transduction. To address this issue, we performed a cell-based transcriptional reporter assay using reporter plasmids bearing VDRE (referred to herein as VDRE-Luc) or SMAD-binding elements (CAGA-Luc) as well as 2 VDR mutants, VDR-mC (D42G/G43S/G46V; ref. 52) and VDR-LBD, both of which lacked DNA-binding ability (Figure 3A and see Methods). Expression of VDR-mC or VDR-LBD in HEK293 cells did not induce the transcription of VDRE-Luc (Figure 3A). In contrast, $1,25(OH)_2D_3$-dependent suppression of TGF-β–SMAD signal transduction was observed in cells that expressed VDR-mC or VDR-LBD as well as VDR (Figure 3A). These

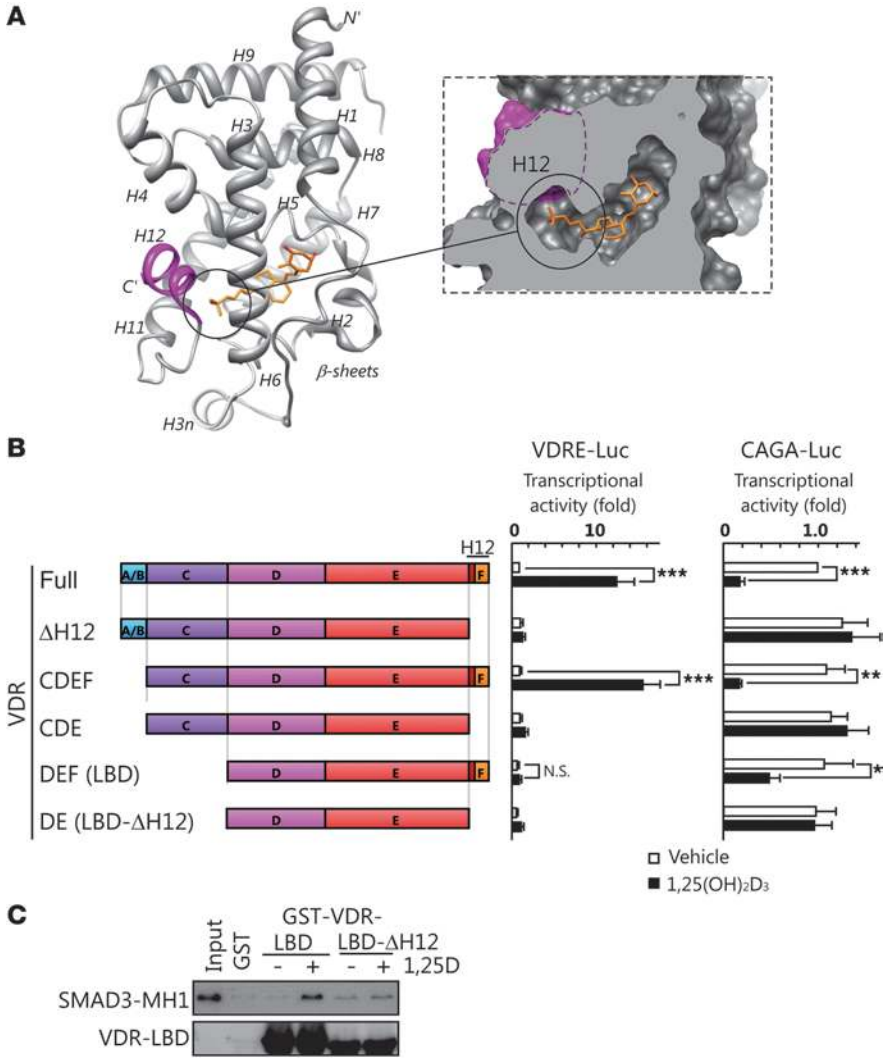


**Figure 4**
H12 in VDR is required for the suppression of TGF-β–SMAD signal transduction. (**A**) The VDR-LBD and ligand-binding pocket are shown in the crystal structure of VDR complexed with $1,25(OH)_2D_3$ (PDB: 1DB1). An enlarged view of the ligand-binding pocket is also shown. H12 is shown in magenta; $1,25(OH)_2D_3$ is shown in orange. (**B**) H12 is necessary for transactivation and suppression of TGF-β signal transduction. VDR truncations are as follows: full, 1–427 aa; ΔH12, 1–403 aa; CDEF, 20–427 aa; CDE, 20–403 aa; DEF (LBD), 110–427 aa; DE (LBD-ΔH12), 110–403 aa. HEK293 cells were transfected with plasmids encoding ALK5 TD and the indicated VDR mutants and the reporter plasmids VDRE-Luc or CAGA-Luc. After culturing transfected cells with or without $1,25(OH)_2D_3$, cell extracts were analyzed using luciferase assay. (**C**) H12 is necessary for SMAD3 binding. Purified recombinant His-tagged SMAD3-MH1 was incubated with GST-VDR-LBD or GST-VDR-LBD-ΔH12 in the presence or absence of $1,25(OH)_2D_3$, after which the mixtures were examined by in vitro pulldown assay. $^*P < 0.05$; $^{**}P < 0.01$; $^{***}P < 0.001$.

results indicate that the DNA-binding ability and induction of transactivation of VDR are not necessary for the $1,25(OH)_2D_3$-dependent inhibition of TGF-β–SMAD signal transduction.

Because VDR-mediated transcription was not necessary for $1,25(OH)_2D_3$-dependent inhibition of TGF-β–SMAD signal transduction, we next tested the interaction between VDR and SMAD proteins. In vitro binding assays showed that SMAD3, but not SMAD2 or SMAD4, bound to the VDR-LBD in a $1,25(OH)_2D_3$-dependent manner (Figure 3B and Supplemental Figure 1D). To identify the regions responsible for VDR binding in SMAD3, we generated mad homology 1 (MH1), MH1 plus linker (MH1L), and MH2 domains of SMAD3 (Figure 3C). In the binding assay, we identified the domain SMAD3-MH1 as the region that specifically bound to the VDR-LBD (Figure 3C and Supplemental Figure 1E).

Since SMAD3-MH1 possessed DNA binding ability, we investigated whether VDR and $1,25(OH)_2D_3$ affect binding of SMAD3 to DNA. EMSA showed that SMAD3-MH1 formed a complex with a DNA probe containing a SMAD3-binding element, but formation of this complex was prevented in the presence of both VDR-LBD and $1,25(OH)_2D_3$ (Figure 3D). These results indicated that the VDR binds to SMAD3-MH1, thereby inhibiting the ability of SMAD3 to bind to DNA.

*The C-terminal H12 is necessary for VDR-mediated suppression of TGF-β–SMAD signal transduction*. In classical genomic action, VDR binds to specific response elements (i.e., VDRE) and regulates transcription of target genes. In contrast, our results indicated that VDR suppresses TGF-β–SMAD signal transduction by binding to SMAD3. Therefore, the classical genomic action of VDR may not be involved in the suppression of renal fibrosis by $1,25(OH)_2D_3$. To test this possibility, we attempted to generate VDR ligands able to inhibit TGF-β–SMAD signal transduction without activating VDR-mediated transcription.

We first examined the structural underpinnings of VDR-mediated inhibition of TGF-β–SMAD signal transduction. The structure of the $1,25(OH)_2D_3$–VDR-LBD complex has previously been examined using X-ray crystallography (34). In this complex, $1,25(OH)_2D_3$ associates with and stabilizes H12 of the VDR-LBD (Figure 4A) to facilitate interactions with coactivators, including SRC-1 (35). Because H12 has a critical role for VDR-mediated transcription, we examined the effect of H12 on VDR-dependent suppression of TGF-β–SMAD signal transduction. We confirmed that the transcriptional activity of the VDR was abolished by deleting H12 (VDR-ΔH12; Figure 4B). H12 deletion also abolished the inhibition of TGF-β–dependent transcription, as shown using

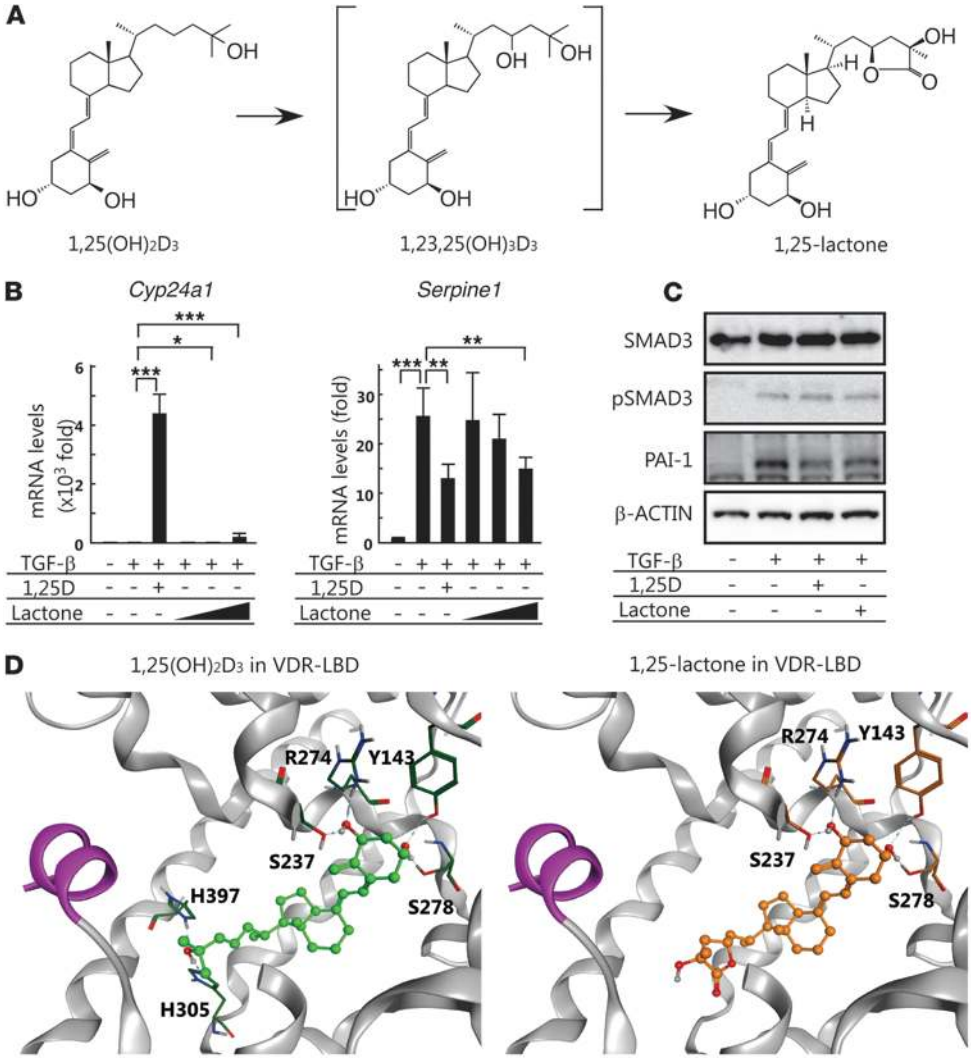


**Figure 5**
Endogenous vitamin D metabolite suppresses TGF-β–SMAD signal transduction. (**A**) The C-23 $1,25(OH)_2D_3$ metabolic pathway. (**B**) TCMK-1 cells were cultured in the presence or absence of 5 ng/ml TGF-β, 10 nM $1,25(OH)_2D_3$, or 0.01, 0.1, or 1 μM 1,25-lactone for 8 hours, and *Cyp24a1* and *Serpine1* mRNA levels were determined by qPCR. (**C**) TCMK-1 cells were treated with or without 5 ng/ml TGF-β and 10 nM $1,25(OH)_2D_3$ or 1 μM 1,25-lactone. SMAD3, pSMAD3, PAI-1, and β-actin levels were assessed by Western blotting. (**D**) Binding of 1,25-lactone to agonistic VDR. 1,25-lactone was docked in the ligand-binding pocket of the VDR-LBD in complex with $1,25(OH)_2D_3$ (PDB: 1DB1) using MOE. 1,25-lactone and $1,25(OH)_2D_3$ are shown with residues forming hydrogen bonds. H12 is shown in magenta. Residues between A231 and Y236 have been omitted for clarity. $^*P < 0.05$; $^{**}P < 0.01$; $^{***}P < 0.001$.

VDR-ΔH12 compared with full-length VDR. Similar results were obtained by deleting H12 from VDR-LBD (VDR-LBD-ΔH12). Consistent with the results of transcription assays (Figure 4B), in vitro pulldown experiments showed that VDR-LBD-ΔH12 did not bind to SMAD3-MH1 (Figure 4C and Supplemental Figure 1F). These results demonstrated that the H12 region of the VDR-LBD is required for interaction with SMAD3.

*An endogenous vitamin D metabolite induces weak stimulation of VDR transcription, but suppression of TGF-β–SMAD signal transduction.* Because H12 is required to interact with both SMAD3 and coactivators, VDR ligands that specifically inhibit TGF-β–SMAD signal transduction might associate with H12 and create a conformation specific for interaction with SMAD3. We therefore focused on 1α,25-dihydroxyvitamin $D_3$-26,23-lactone (1,25-lactone), a metabolite of $1,25(OH)_2D_3$ that has been detected in human serum (Figure 5A and ref. 53). Since 1,25-lactone has a γ-butyrolactone ring, it may affect the conformation of H12 differently than $1,25(OH)_2D_3$ (Figure 5A). qPCR analyses indicated that, in contrast to $1,25(OH)_2D_3$, the same dose of 1,25-lactone did not induce *Cyp24a1* expression, and higher 1,25-lactone doses induced weak but detectable expression (Figure 5B). Conversely, this higher dose of 1,25-lactone was sufficient to inhibit production of *Serpine1* mRNA expression as strong as $1,25(OH)_2D_3$ (Figure 5B). Western blot analysis also confirmed that PAI-1 protein levels were decreased by the higher dose of 1,25-lactone (Figure 5C and Supplemental Figure 1G). In addition, TGF-β–induced pSMAD3 levels were not affected by 1,25-lactone (Figure 5C and Supplemental Figure 1G). These observations suggest that the γ-butyrolactone ring of 1,25-lactone induces conformation in H12 that preferentially facilitates interactions with SMAD3 rather than with coactivators.

A previous study of the structure of the $1,25(OH)_2D_3$–VDR-LBD complex (34) revealed that VDR residues His305 and His397 form a hydrogen bond network with the 25-hydroxyl group of $1,25(OH)_2D_3$, thus stabilizing the conformation of H12 in the LBD (Figure 5D and Supplemental Figure 4). A molecular docking simulation study of the 1,25-lactone–VDR-LBD complex revealed that VDR residues His305 and His397 associate with 1,25-lactone in a different manner than with $1,25(OH)_2D_3$: His305 and His397 form hydrophobic interactions, which are weaker than hydrogen bonds, with 1,25-lactone (Figure 5D and Supplemental Figure 4). Conversely, the vitamin D secosteroid backbone of 1,25-lactone — which is also a structural feature of $1,25(OH)_2D_3$ — interacts with the VDR-LBD in a configuration similar to that of $1,25(OH)_2D_3$

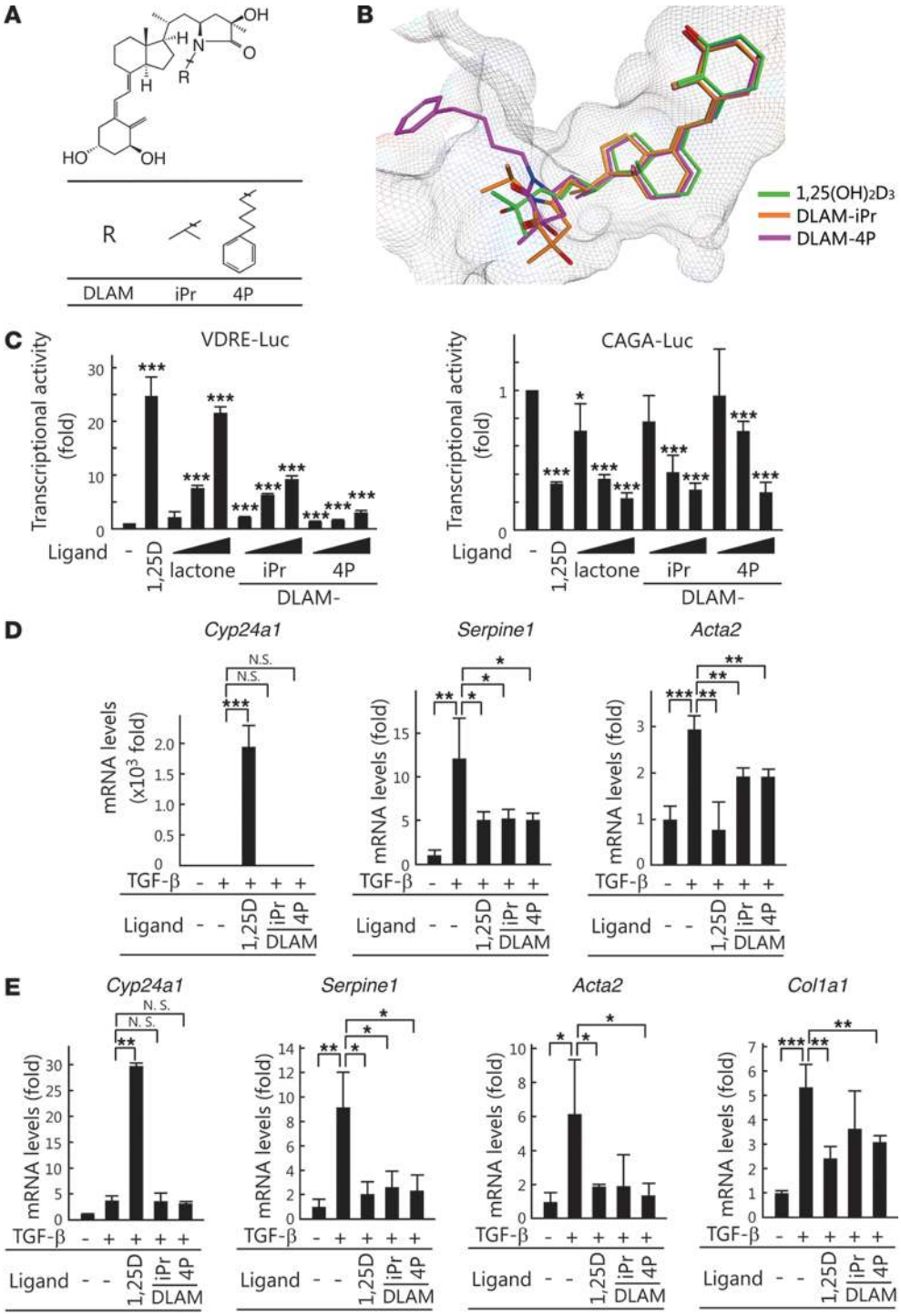


**Figure 6**

DLAM derivatives that suppress TGF-β–dependent transcription without VDR transactivation. (**A**) DLAM derivatives, DLAM-iPr and DLAM-4P, used in this study. (**B**) Binding of DLAM-iPr and DLAM-4P to agonistic VDR. The DLAM derivatives were docked into the ligand-binding pocket in the VDR-LBD complexed with $1,25(OH)_2D_3$ (PDB: 1DB1) using MOE. The ligand-binding pocket of VDR-LBD-ΔH12 is represented as a mesh model. (**C**) Dose responses of DLAM-iPr and DLAM-4P. Plasmids encoding ALK5 TD and VDR were transfected with reporter plasmids VDRE-Luc and CAGA-Luc into HEK293 cells. After culturing transfected cells with or without $1,25(OH)_2D_3$ (10 nM), 1,25-lactone (0.01, 0.1, or 1 μM), or DLAM derivatives (0.01, 0.1, or 1 μM) for 24 hours, cell extracts were analyzed in luciferase assays. (**D**) TCMK-1 cells were cultured in the presence or absence of 5 ng/ml TGF-β and 10 nM $1,25(OH)_2D_3$, 1 μM DLAM-iPr, or 1 μM DLAM-4P. *Cyp24a1*, *Serpine1*, and *Acta2* mRNA levels were determined using qPCR. (**E**) Kidney fibroblasts were isolated and cultured in the presence or absence of 5 ng/ml TGF-β and 10 nM $1,25(OH)_2D_3$, 1 μM DLAM-iPr, or 1 μM DLAM-4P for 8 hours, and *Cyp24a1*, *Serpine1*, *Acta2*, and *Col1a1* mRNA levels were determined using qPCR. $^*P < 0.05$; $^{**}P < 0.01$; $^{***}P < 0.001$.

(Figure 5D and Supplemental Figure 4). These data suggest that 1,25-lactone induces a conformational change in H12 that stimulates partial VDR-mediated transcription, yet also inhibits TGF-β–SMAD signal transduction.

*DLAM derivatives suppress TGF-β–SMAD signal transduction without activating VDR-mediated transcription.* Based on the results of our molecular docking simulation study, we attempted to develop compounds that would specifically inhibit TGF-β–SMAD signal transduction via VDR without VDR-mediated transcription activation. Given the structure of 1,25-lactone and its effect on VDR activity, we hypothesized that further modification of 1,25-lactone to directly affect the conformation of H12 may decrease stimulation of VDR-mediated transcription, but still inhibit TGF-β–SMAD signal transduction. To validate our hypothesis, we focused on 1,25-lactone–mimicking VDR ligands, i.e., DLAM derivatives (54). Previously, we showed that DLAMs suppress the promyelocytic leukemia cell differentiation induced by $1,25(OH)_2D_3$ (54). More interestingly, these derivatives possess a variety of substituents on the nitrogen

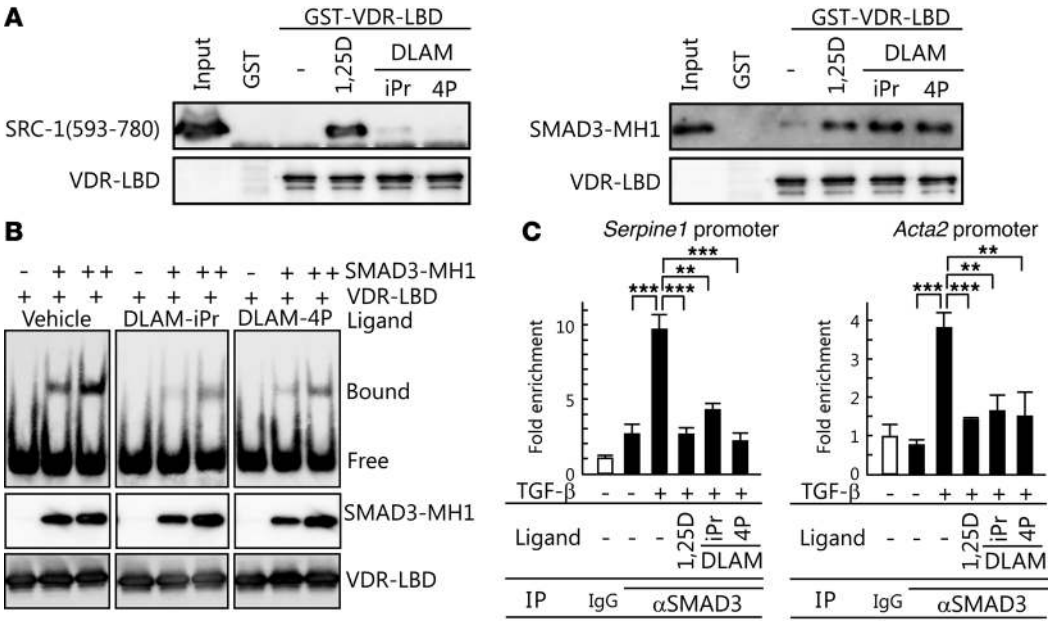


**Figure 7**

DLAM derivatives suppress TGF-β–dependent transcription by inhibiting the DNA binding of SMAD3. (**A**) Analysis of the interaction between the DLAM-bound VDR and SRC-1 or SMAD3. Flag-tagged SRC-1 (aa 593–730) was expressed in HEK293 cells, and the cell extracts or purified recombinant His-tagged SMAD3-MH1 (aa 1–132) were incubated with GST-VDR-LBD in the presence or absence of $1,25(OH)_2D_3$. Mixtures were then analyzed by in vitro pulldown assay. (**B**) DLAM-iPr and DLAM-4P interfere with binding of SMAD3 to the SMAD3-binding element. Purified recombinant SMAD3-MH1 and VDR-LBD were incubated with a DNA probe containing the SMAD3-binding element in the presence or absence of the indicated ligands, and binding of SMAD3-MH1 to the probe was analyzed by EMSA (top). Protein levels were aslo assessed by Western blotting (middle and bottom). (**C**) Inhibition of TGF-β–dependent SMAD3 recruitment to the *Serpine1* and *Acta2* promoters by DLAM-iPr and DLAM-4P. TCMK-1 cells were cultured in the presence or absence of 5 ng/ml TGF-β, 10 nM $1,25(OH)_2D_3$, 1 μM DLAM-iPr, or 1 μM DLAM-4P. ChIP assays were performed with control IgG or anti-SMAD3 antibodies. Immunoprecipitated DNA was examined by qPCR with primers specific for the *Serpine1* or *Acta2* promoter. Samples were normalized to input DNA level. $^{**}P < 0.01$; $^{***}P < 0.001$.

atom of the lactam skeleton at the position of $1,25(OH)_2D_3$ side chain. We expected the substituents in these compounds to have steric effects on the conformation of H12; therefore, we examined the effects of DLAM-iPr and DLAM-4P (Figure 6A).

Similar to the case of 1,25-lactone, molecular docking analyses of DLAM-iPr– and DLAM-4P–VDR-LBD complexes revealed that the vitamin D secosteroid backbones of these DLAM molecules interact with the VDR-LBD in a configuration similar to $1,25(OH)_2D_3$ (Figure 6B). In addition, the simulation study showed that VDR-LBD residues His305 and His397 do not form a hydrogen bond network, as seen with $1,25(OH)_2D_3$ (Supplemental Figure 5). Furthermore, we confirmed that the DLAM-iPr and DLAM-4P substituents are directed toward H12, and that the long substituent of DLAM-4P apparently interferes with the agonistic position of H12 in the VDR-LBD (Figure 6B).

In a transcription assay, although 1,25-lactone activated VDR-mediated transcription from VDRE-Luc, DLAM-iPr and DLAM-4P showed relatively weak stimulation of VDR-mediated transcription and marked inhibition of TGF-β–SMAD signal transduction (Figure 6C and Supplemental Figure 6). In particular, 1,25-lactone appeared to have a markedly high effect on VDR transcriptional activity (compare Figure 6C with Figure 5B), because of differences in the sensitivities of the VDR activity to ligands between the transcription reporter and qPCR assays. In TCMK-1 cells, DLAM-iPr and DLAM-4P abrogated mRNA expression of TGF-β–dependent *Serpine1* and *Acta2* without inducing *Cyp24a1* (Figure 6D). Similar to TCMK-1 cells, DLAM compounds decreased *Serpine1* expression in HK-2 cells (Supplemental Figure 3, A and B). In mouse fibroblasts, TGF-β–induced expression of *Serpine1*, *Acta2*, and *Col1a1* mRNA was suppressed by DLAM-iPr and DLAM-4P without inducing *Cyp24a1* expression (Figure 6E). These data suggest that both the lactam skeleton and the substituents of DLAM-iPr and DLAM-4P modulate the conformation of H12, leading to a nonagonistic state in the VDR.

To confirm that the DLAM derivatives induce the specific conformation of VDR to interact with SMAD3, we performed in vitro pulldown assays with glutathione S-transferase–bound VDR-LBD (GST-VDR-LBD) and the transcriptional cofactor SRC-1 (aa 593–780) or SMAD3-MH1 (aa 1–132). Unlike $1,25(OH)_2D_3$, DLAM-iPr and DLAM-4P did not induce formation of a complex between the VDR and SRC-1 (Figure 7A and Supplemental Figure 1H). In contrast, similar to $1,25(OH)_2D_3$, the DLAM derivatives did induce formation of a complex between the VDR and SMAD3-MH1 (Figure 7A and Supplemental Figure 1H). These data suggest that DLAMs alter the apo-state of the VDR-LBD into a specific nonagonistic state, and that SMAD3 can bind to either the $1,25(OH)_2D_3$-induced agonistic state or the DLAM derivative–induced nonagonistic state of the VDR. We examined whether DLAM-iPr and DLAM-4P can suppress TGF-β–SMAD signal transduction by inhibiting the binding of SMAD3 to DNA via the VDR. EMSA experiments showed that DLAM-iPr and DLAM-4P reduced the binding of SMAD3-MH1 to DNA (Figure 7B). Moreover, ChIP experiments confirmed

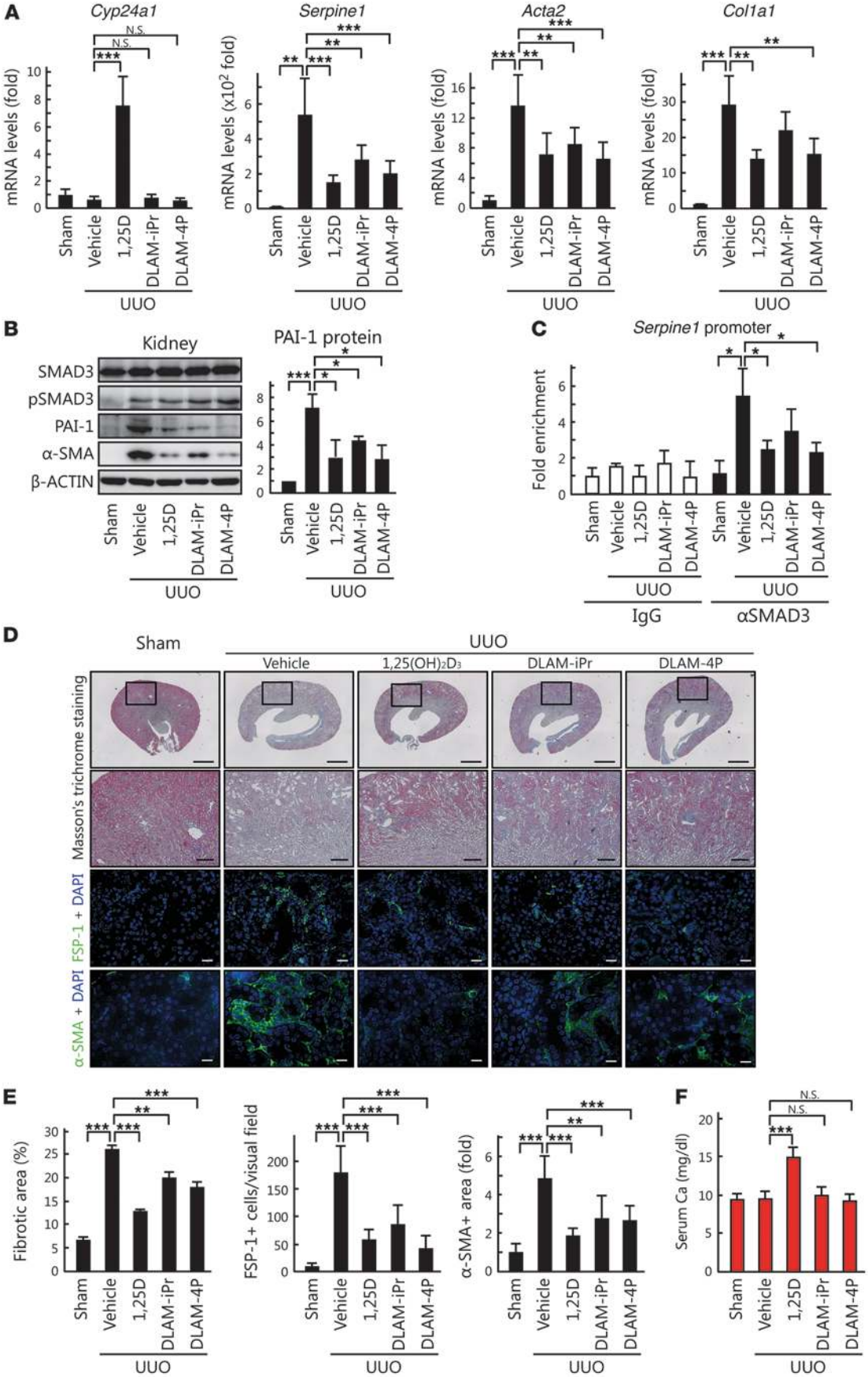
A
Cyp24a1
Serpine1
Acta2
Col1a1
mRNA levels (fold)
mRNA levels (x10² fold)
N.S.
Sham
Vehicle
1,25D
DLAM-iPr
DLAM-4P
UUO
B
Kidney
SMAD3
pSMAD3
PAI-1
α-SMA
β-ACTIN
PAI-1 protein
C
Serpine1 promoter
Fold enrichment
IgG
αSMAD3
D
Sham
UUO
Vehicle
1,25(OH)2D3
DLAM-iPr
DLAM-4P
Masson's trichrome staining
FSP-1 + DAPI
α-SMA + DAPI
E
Fibrotic area (%)
FSP-1+ cells/visual field
α-SMA+ area (fold)
F
Serum Ca (mg/dl)
N.S.

**Figure 8**
DLAM-iPr and DLAM-4P suppress tubulointerstitial sclerosis without inducing hypercalcemia in UUO mice. (**A**) DLAM-iPr and DLAM-4P suppress the expression of profibrotic genes. *Cyp24a1*, *Serpine1*, *Acta2*, and *Col1a1* mRNA levels were determined by qPCR using RNA isolated from sham-operated ($n$ = 4) or UUO kidneys of mice treated with vehicle ($n$ = 7), $1,25(OH)_2D_3$ ($n$ = 8), DLAM-iPr ($n$ = 9), or DLAM-4P ($n$ = 9). (**B**) Western blot analysis of SMAD3, pSMAD3, PAI-1, α-SMA, and β-actin in UUO and sham-operated mouse kidneys. Quantification of PAI-1 protein levels ($n$ = 3 per treatment group; see Methods) is also shown. (**C**) DLAM-iPr and DLAM-4P inhibited SMAD3 recruitment to the *Serpine1* promoter in the kidneys. Kidney samples from UUO or sham-operated mice were subjected to ChIP assay with control IgG or anti-SMAD3 antibodies. Immunoprecipitated DNA was examined using qPCR with primers specific for the *Serpine1* promoter. Samples were normalized to input DNA level ($n$ = 3 per group). (**D**) Representative photomicrographs of Masson's trichrome staining (top row, whole kidney; second row, magnified view of boxed region, enlarged ×4.37), FSP-1– (third row), and α-SMA–specific immunofluorescence staining (bottom row) of kidney sections from sham-operated or UUO mice injected with vehicle, $1,25(OH)_2D_3$, DLAM-iPr, or DLAM-4P. Scale bars: 1.0 mm (top row); 200 μm (second row); 20 μm (bottom 2 rows). (**E**) Fibrotic areas ($n$ = 3 per group), FSP-1–positive cells ($n$ = 12 per group), and α-SMA–positive areas ($n$ = 8 per group) in stained kidney sections. (**F**) Serum calcium concentration. $^*P < 0.05$; $^{**}P < 0.01$; $^{***}P < 0.001$.

that the binding of SMAD3 to the *Serpine1* and *Acta2* promoters was inhibited by both DLAM-iPr and DLAM-4P in TCMK-1 cells (Figure 7C). In HK-2 cells, SMAD3 binding to the *Serpine1* promoter was inhibited by these compounds (Supplemental Figure 3C).

*DLAM derivatives suppress renal fibrosis without inducing hypercalcemia*. To examine whether the suppression of renal fibrosis by $1,25(OH)_2D_3$ is due to the inhibition of SMAD signaling by VDR, we tested the effect of DLAM-iPr and DLAM-4P on renal fibrosis caused by UUO. In mouse kidney, DLAM-iPr and DLAM-4P did not increase the level of *Cyp24a1* mRNA, whereas $1,25(OH)_2D_3$ did (Figure 8A). In contrast, administration of DLAM-iPr and DLAM-4P significantly reduced *Serpine1*, *Acta2*, and *Col1a1* mRNA levels in UUO kidneys (Figure 8A). Consistent with these results, UUO-induced PAI-1 and α-SMA protein expression was also inhibited by DLAM-iPr and DLAM-4P (Figure 8B and Supplemental Figure 1I). While the level of pSMAD3 was not affected by the VDR ligands in UUO mice (Figure 8B and Supplemental Figure 1I), ChIP experiments revealed suppressed binding of SMAD3 to the *Serpine1* promoter in response to DLAM-iPr and DLAM-4P treatment (Figure 8C), confirming the inhibition of TGF-β–SMAD signal transduction. Consistent with these results, both DLAM-iPr and DLAM-4P led to a decrease in the size of the area stained with aniline blue, anti–FSP-1 antibody, or anti–α-SMA antibody in UUO kidneys (Figure 8, D and E). There was no appreciable increase in serum calcium in mice treated with DLAM-iPr or DLAM-4P (Figure 8F), in concordance with the inability of these ligands to induce VDR-mediated transcription.

Several studies have shown that vitamin D analogs are renoprotective in experimental animal models with renal diseases. One of these analogs, paricalcitol, is a VDR agonist and is used as a drug for prevention and treatment of secondary hyperparathyroidism associated with chronic renal failure. Preclinical studies have shown that paricalcitol induces less hypercalcemia than $1,25(OH)_2D_3$ (55). We therefore compared paricalcitol and DLAM compounds in terms of their VDR-agonistic, fibrotic, and hypercalcemic effects in UUO kidneys. Unlike DLAMs, mRNA expression of *Cyp24a1* was elevated by paricalcitol (Figure 8A and Supplemental Figure 7). In contrast, similar to DLAMs, paricalcitol decreased *Acta2* and *Col1a1* mRNA levels (Supplemental Figure 7) as well as the size of the area stained with aniline blue, anti–FSP-1 antibody, or anti–α-SMA antibody (Supplemental Figure 8). Paricalcitol did not decrease the typical level of the TGF-β target gene *Serpine1* in UUO kidneys (Supplemental Figure 7). More importantly, unlike DLAMs, paricalcitol significantly elevated serum calcium levels compared with vehicle in our experimental condition (Supplemental Figure 9).

Next, we tested DLAM-iPr and DLAM-4P using an alternative renal fibrosis model, i.e., folic acid–induced nephropathy (56). Mice were intraperitoneally injected with folic acid after administration of vehicle or DLAM derivatives and analyzed after 14 and 129 days (short- and long-term analysis, respectively). In the short-term analysis, mRNA levels of *Tgfb1*, *Serpine1*, *Acta2*, and *Col1a1* increased in mice injected with folic acid (Supplemental Figure 10A). In agreement with the results of the UUO model, mRNA levels of *Serpine1*, *Acta2*, and *Col1a1* decreased in response to $1,25(OH)_2D_3$, DLAM-iPr, and DLAM-4P, whereas *Tgfb1* mRNA was not affected (Supplemental Figure 10A). Similar results were observed in Western blot analyses, in which PAI-1 and α-SMA protein levels significantly decreased in response to $1,25(OH)_2D_3$, DLAM-iPr, and DLAM-4P, whereas SMAD3 and pSMAD3 levels were not affected (Supplemental Figure 10B). In the long-term analysis, *Serpine1*, *Acta2*, and *Col1a1* expression decreased in response to treatment with DLAM-iPr or DLAM-4P (Figure 9A). Masson's trichrome and immunohistochemical staining of kidneys as well as measurement of serum creatinine showed significant inhibition of progressive fibrosis and renal failure in DLAM-iPr– and DLAM-4P–treated mice (Figure 9, B–D). Unlike $1,25(OH)_2D_3$, DLAM-iPr and DLAM-4P did not increase serum calcium levels in the short-term analysis. Moreover, even in the long-term analysis, DLAMs only slightly increased the serum calcium level (Figure 9E).

Taken together, these results show that DLAM-iPr and DLAM-4P reduce renal fibrosis by inhibiting TGF-β–SMAD signal transduction, but do not induce hypercalcemia via VDR transactivation. Therefore, these synthetic ligands may be good candidates for use in treating renal fibrosis.

## Discussion

TGF-β plays a crucial role in the maintenance of tissue homeostasis. Disrupted TGF-β signal transduction has been implicated in many human diseases, including neoplastic, autoimmune, fibrotic, and cardiovascular conditions as well as tumor progression. In the present study, we demonstrated that the natural vitamin D metabolite $1,25(OH)_2D_3$ suppressed TGF-β–SMAD signal transduction in fibrogenesis of the kidneys. In addition, we observed that $1,25(OH)_2D_3$-bound VDR interacted directly with SMAD3-MH1, which contains a DNA-binding motif. This interaction decreased binding of SMAD3 to DNA and inhibited TGF-β–SMAD signal transduction. Using DLAM-iPr and DLAM-4P, which specifically inhibit TGF-β–SMAD signal transduction without activation of classical VDR-mediated transcription, we demonstrated that VDR suppresses renal fibrosis by inhibiting TGF-β–SMAD signal transduction; thus, VDR suppresses renal fibrosis via a nonclassical pathway.

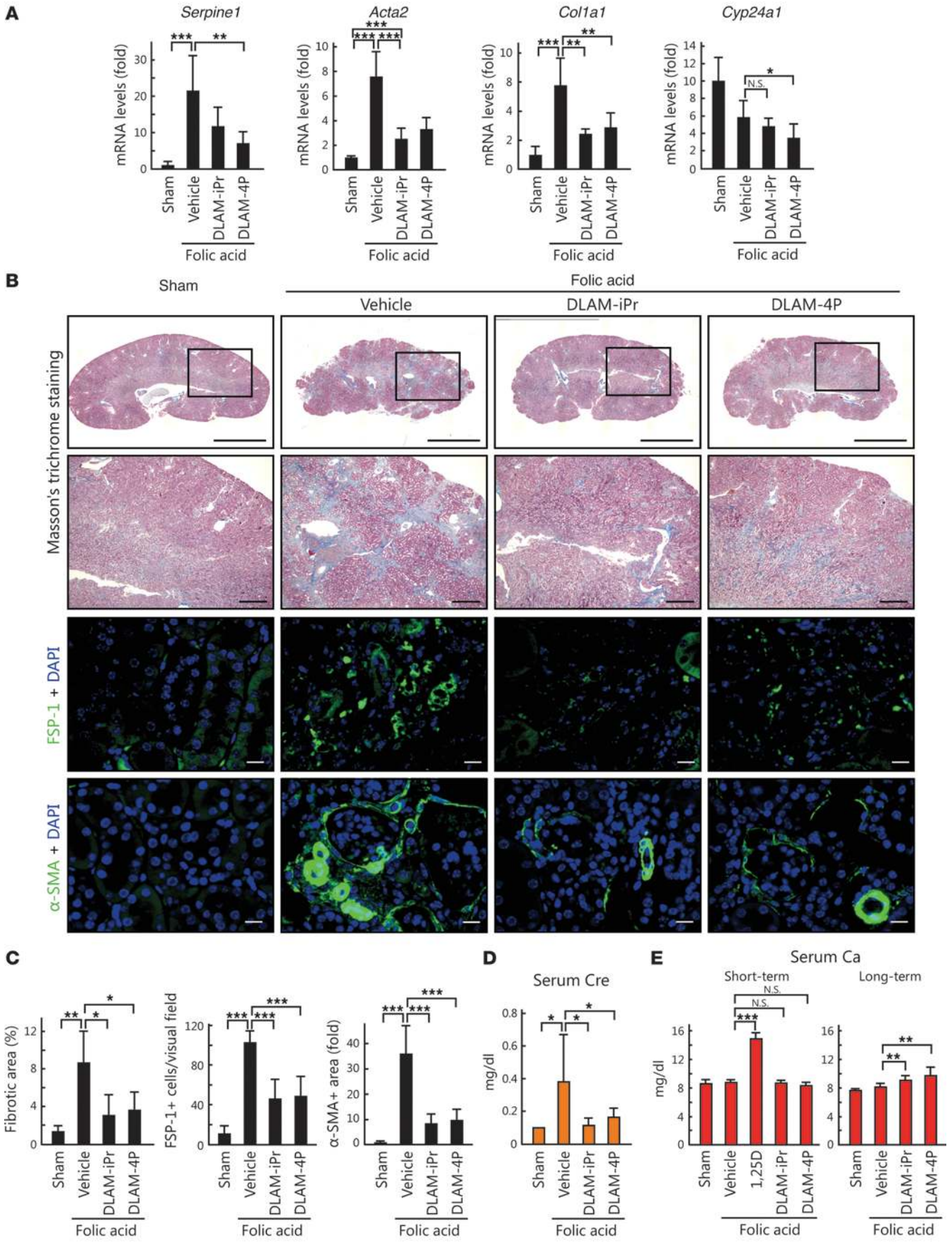
A
Serpine1
Acta2
Col1a1
Cyp24a1
mRNA levels (fold)
Sham
Vehicle
DLAM-iPr
DLAM-4P
Folic acid
N.S.
B
Sham
Folic acid
Vehicle
DLAM-iPr
DLAM-4P
Masson's trichrome staining
FSP-1 + DAPI
α-SMA + DAPI
C
Fibrotic area (%)
FSP-1+ cells/visual field
α-SMA+ area (fold)
D
Serum Cre
mg/dl
E
Serum Ca
Short-term
Long-term
1,25D

**Figure 9**
DLAM-iPr and DLAM-4P ameliorate folic acid–induced nephropathy. (**A**) DLAM-iPr and DLAM-4P suppress the expression of profibrotic genes 129 days after folic acid injection. We prepared RNA from kidneys of mice treated with folic acid and the indicated ligands, and *Cyp24a1*, *Serpine1*, *Acta2*, and *Col1a1* mRNA levels were examined by qPCR. (**B**) Representative photomicrographs of Masson's trichrome staining (top row, whole kidney; second row, magnified view of boxed region, enlarged ×3.24), FSP-1– (third row), and α-SMA–specific immunofluorescence staining (bottom row) of kidney sections from mice that received folic acid (vehicle). 3 days after injection, mice were treated with vehicle, 0.6 μg/kg/d $1,25(OH)_2D_3$, 60 μg/kg/d DLAM-iPr, or 60 μg/kg/d DLAM-4P by continuous infusion from osmotic pumps. Mice were analyzed 129 days after folic acid injection. Scale bars: 3.0 mm (top row); 500 μm (second row); 20 μm (bottom 2 rows). (**C**) Fibrotic area ($n = 4$ per group), FSP-1–positive cells in stained sections ($n = 10$ per group), and α-SMA–positive area ($n = 10$ per group). (**D** and **E**) Serum creatinine (**D**) and calcium (**E**) concentrations. Short-term, 14 days; Long-term, 129 days. *$P < 0.05$; **$P < 0.01$; ***$P < 0.001$.

Vitamin D undergoes a sequential 2-step metabolism in the liver and kidneys to form $1,25(OH)_2D_3$, which is thought to be the most potent metabolite of vitamin D. $1,25(OH)_2D_3$ regulation of VDR-mediated classical genomic actions in target organs such as intestine, bone, and parathyroid glands plays an important role in the in vivo maintenance of calcium homeostasis. Although other effects of $1,25(OH)_2D_3$ have been reported, including inhibition of cell proliferation, induction of cell differentiation, modulation of immune responses, stimulation of insulin secretion, and various neurological effects, the detailed action mechanisms of these effects remain to be determined. In this study, we found that $1,25(OH)_2D_3$-bound VDR directly interacted with SMAD3 and regulated SMAD-mediated signal transduction independent of its classical genomic action. Since $1,25(OH)_2D_3$ has multiple effects beyond the maintenance of calcium homeostasis mentioned above, it may regulate these effects through nonclassical action of VDR.

Although vitamin D is metabolized into at least 30 known metabolites, $1,25(OH)_2D_3$ alone has been shown to be capable of producing most of the biological responses attributed to vitamin D; however, our results suggest that another vitamin D metabolite, 1,25-lactone, is also biologically effective. 1,25-lactone has been isolated and identified as a metabolite of $1,25(OH)_2D_3$ in sera from animals administered pharmacologic doses of $1,25(OH)_2D_3$, as well as from humans under physiological conditions (57, 58). Although the precise metabolic half-life of 1,25-lactone has not been determined, it appears to be longer than that of $1,25(OH)_2D_3$ (59). Our results revealed that $1,25(OH)_2D_3$ attenuated renal fibrosis by inhibiting TGF-β–SMAD signal transduction and that 1,25-lactone also had an inhibitory effect on TGF-β–SMAD signal transduction. From these observations, it appears that 1,25-lactone is not merely a waste metabolite of $1,25(OH)_2D_3$, but is a natural compound with specific biological functions. Because $1,25(OH)_2D_3$ fully activated VDR-mediated transcription and 1,25-lactone showed minimal activity with an inhibitory effect on TGF-β–SMAD signal transduction, the metabolism of $1,25(OH)_2D_3$ to form 1,25-lactone may involve shifting of VDR function from the classical genomic action to a nonclassical action.

Our results indicate that $1,25(OH)_2D_3$ suppresses renal fibrosis through inhibition of TGF-β–SMAD signal transduction, whereas previous studies have examined the effect of VDR agonists on a number of signaling pathways as a means of inhibiting renal fibrosis. For example, VDR agonists have been reported to inhibit the renin-angiotensin system (41, 43, 45, 48), reduce NF-κB–dependent transcription (44, 46, 47), and increase HGF production (42), which antagonizes TGF-β binding to the cell surface receptors. Attenuation of renin-angiotensin signaling and NF-κB–mediated inflammatory networks results in downregulation of *Tgfb1* mRNA synthesis and leads to reduced phosphorylation of SMAD2 and SMAD3. In addition, increased HGF levels reduce phosphorylation of SMADs. In the UUO and folic acid–induced mouse models, we observed that *Tgfb1* mRNA levels and SMAD3 phosphorylation were not affected by $1,25(OH)_2D_3$. In addition, similar effects were observed with DLAM-iPr and DLAM-4P, neither of which stimulated VDR-mediated transcription. Our observations indicate that $1,25(OH)_2D_3$, DLAM-iPr, and DLAM-4P suppress renal fibrosis primarily via inhibition of TGF-β–SMAD signal transduction. However, we cannot exclude the possibility of multiple suppressive effects of VDR on renal fibrosis.

Given its almost universal appearance in chronic kidney disease, renal fibrosis is a promising treatment target. During the fibrotic process, a preferential target for therapy is the fundamental cell responsible for the exaggerated production and deposition of ECM. Interstitial myofibroblasts have been widely regarded as the major source of interstitial ECM. In addition, renal fibrosis is often associated with inflammatory infiltration of monocytes and macrophages, which are essential for the regulation of immune responses and the development of inflammation. Therefore, understanding the origin of these cells in kidney undergoing fibrosis is of great interest in chronic kidney disease; however, it is still controversial. In this study, we clearly showed that α-SMA–positive myofibroblasts and FSP-1–positive macrophages were significantly reduced by treatment with DLAM compounds and that DLAMs decreased expression levels of TGF-β–induced fibrotic genes in mouse kidney fibroblasts. From these results, we concluded that renal fibroblasts and/or macrophages, as well as myofibroblasts, are the targets of DLAM-iPr and DLAM-4P. We believe that better understanding of these potent target cells for DLAM compounds might lead to more efficacious treatments and that new insights into the onset and progression mechanisms of the underlying diseases offer the promise of improved approaches to therapy for renal fibrosis.

It has been reported that $1,25(OH)_2D_3$ and VDR regulate intestinal calcium/phosphate absorption and remodeling of bone to maintain calcium homeostasis via its genomic action. Furthermore, the ligand and receptor stimulate rapid responses (and corresponding nongenomic actions) in the intestine (rapid $Ca^{2+}/Cl^-$ absorption), pancreatic β cells (insulin secretion), endothelial cells (cell migration), osteoblasts (exocytosis), and Sertoli cells (exocytosis or secretion) (39). Although $1,25(OH)_2D_3$ affects cell proliferation and differentiation, it remains unclear how this ligand regulates these biological events via its receptor. Vitamin D deficiency is associated with skeletal disease, hyperparathyroidism, and chronic diseases (60), which affects exogenous compounds such as DLAMs; therefore, there is an increased risk of diseases related to vitamin D deficiency after inhibiting the binding between $1,25(OH)_2D_3$ and VDR or pleiotropic VDR actions. However, our present study showed that DLAMs ameliorated renal fibrosis without altering serum calcium levels or inducing hypercalcemia. Furthermore, we found that DLAM-treated mice did not exhibit any abnormalities related to impaired vitamin D metabolism, such as reduced body weight or behavioral disorders, suggesting the absence of detectable adverse effects of DLAMs. Thus, we conclude that DLAM-iPr and

DLAM-4P have little effect on normal vitamin D signaling via VDR in vivo. However, we cannot exclude the possibility that DLAMs induce effects via rapid VDR response or other actions.

TGF-β–SMAD signal transduction is reported to be involved in several disorders, including cardiac, hepatic, skin, pulmonary, and renal fibrosis. The data from this study suggest that specific stimulation of nonclassical action of VDR by synthetic ligands can suppress tissue fibrosis in several organs. Recently, it has been reported that calcipotriol, an agonist for VDR, prevents carbon tetrachloride–induced liver fibrosis through inhibiting transcriptional activation by SMAD3 (61). In VDR-positive hepatocyte stellate cells, TGF-β–SMAD signal transduction causes redistribution of genome-wide VDR binding sites and facilitates VDR binding at SMAD3 profibrotic target genes via TGF-β–dependent chromatin remodeling. In the presence of calcipotriol, VDR binding to the coregulated genes reduces SMAD3 occupancy at these sites, inhibiting fibrosis. Although the ligand-dependent action mechanism of VDR on suppression is somewhat different between liver and kidney, our DLAM compounds may possibly suppress hepatic fibrosis as well as renal fibrosis. Also, our results may provide a new strategy for development of drugs that do not possess detectable adverse effects. To date, studies have extensively explored the relationship between activation or repression of nuclear receptor–mediated transcription and several human diseases. Since nuclear receptors have long been recognized as transcription factors that bind directly to the genome, drug design for the receptors has typically targeted classical transcriptional regulation. In the present study, we observed that the nonclassical action of VDR plays an important role in protection against renal fibrosis progression. Although it has been observed that some hormonal effects occur regardless of the classical mechanism of nuclear receptor action, the molecular target for the nonclassical effects of nuclear receptors has not been demonstrated conclusively. In addition, although we believe that this nonclassical VDR pathway is involved in protection against renal fibrosis, we suspect that the role of nonclassical pathways of other nuclear receptors in suppressing the progression of human diseases should be studied further. In the case of drug development for targeting the nonclassical pathway of nuclear receptors, a synthetic compound that can selectively stimulate the desired effect, but is dissociated from the classical genomic pathway of the receptor, is required for effective therapy. Our report is the first to demonstrate that it is possible to selectively stimulate a specific activity and to block disease without detectable adverse effects by modifying nuclear receptor ligands. Establishing a general method by which to develop synthetic ligands that stimulate specific nonclassical functions of nuclear receptors is the subject of future studies. Thus, our findings may provide a paradigm for the development of drugs to treat various human diseases by specifically stimulating certain activities of nuclear receptors.

## Methods

Further information can be found in Supplemental Methods.

*Cell culture and transfection*. TCMK-1, HK-2, and HEK293 cells were maintained in DMEM supplemented with 10% FBS. Transfection was performed with PerFectin Transfection Reagent (Gene Therapy Systems) according to the manufacturer's protocols.

*Expression vectors*. DNA fragments encoding VDRs, RXRα, and ALK5 TD were amplified by PCR and cloned into pcDNA3 expression vectors containing sequences coding for FLAG. VDR-mC is a form of VDR bearing 3 amino acid substitutions in the DNA-binding domain (mutation of Asp42, Gly43, and Gly46 to Gly, Ser, and Val, respectively) (52). ALK5 TD is a constitutively active TGF-β type I receptor (mutation of Thr204 to Asp). 3-tandem VDRE sequence (5′-GGTTCACGAGGTTCA-3′) and 9-tandem CAGA sequence (62) were subcloned into a pGL3-Basic reporter plasmid, resulting in VDRE-Luc and CAGA-Luc, respectively.

*Real-time RT-PCR*. 24 hours after seeding cells in phenol red–free DMEM containing 4% charcoal-stripped FBS, we replaced the culture medium with fresh phenol red–free DMEM containing 0.2% charcoal-stripped FBS. After 24 hours of incubation, we added ligands and cultured for 8 hours. We performed qPCR analyses using the Thermal Cycler Dice Real Time System instrument and software (Takara). Primers for qPCR are listed in Supplemental Table 1.

*In vitro GST pulldown assay*. Immobilized GST fusion proteins were preincubated for 30 minutes at 4°C with 10 μM $1,25(OH)_2D_3$ or 1 mM DLAMs in GST-binding buffer (20 mM Hepes-KOH, pH 7.9; 100 mM KCl; 0.2 mM EDTA; 1 mg/ml BSA; 20% glycerol). Immobilized proteins on beads were added to 4 volumes of GST-binding buffer containing 0.01% Tween 20, then incubated at 4°C for 4 hours with 0.5 μg purified His-tagged proteins in the absence or presence of 10 μM $1,25(OH)_2D_3$ or 1 mM DLAMs. After 3 washes in 500 μl GST-binding buffer containing 0.02% Tween 20, elution was performed by incubation in GST-binding buffer containing 0.2% N-lauroylsarkosine (NacalaiTesque) at room temperature for 30 minutes. Samples were resolved by SDS-PAGE and analyzed by Western blotting.

*EMSA*. DNA binding assays were performed essentially as described previously (63), with minor modifications. His-tagged VDR-LBD was preincubated for 30 minutes at 4°C with 10 μM $1,25(OH)_2D_3$ or 1 mM DLAMs in PBS, and 3 volumes of EMSA buffer (20 mM Tris-HCl, pH 7.9; 180 mM KCl; 0.2 mM EDTA; 0.05% NP-40; 0.5 mM PMSF; 1 mM DTT) containing 1 mg/ml BSA, His-tagged SMAD3-MH1, and 1 μM biotinylated SBE oligonucleotide with 10 μM $1,25(OH)_2D_3$ or 1 mM DLAMs were added. The SBE sequence used was 5′-GTATGTCTCAGATGAA-3′ (64). Gel shift assays were carried out at 4°C.

*UUO model*. C57BL/6 mice were purchased from CLEA Japan Inc. We induced kidney injury by UUO. Under 2.5% avertin (NacalaiTesque) anesthesia, the left ureter was ligated at 2 points and cut between the ligatures in order to prevent retrograde urinary tract infection. Sham-operated mice had their ureters manipulated, but not ligated. We initiated subcutaneous injections with $1,25(OH)_2D_3$ (0.3 or 0.6 μg/kg body weight), DLAM-iPr (60 μg/kg body weight), or DLAM-4P (60 μg/kg body weight) every day from the day after UUO until day 7; the other mice received vehicle (propylene glycol). We anesthetized at least 8 mice by intraperitoneal injection of avertin at 7 days. Kidneys were fixed in 4% formaldehyde and embedded in paraffin blocks. For RNA and protein analysis, kidney samples were fresh frozen. We prepared total RNA with Sepazoal (NakaraiTesque) and performed qPCR. Serum calcium was measured with FUJI DRY-CHEM (FUJIFILM) using CA-P III slide.

*Folic acid administration model*. We induced kidney injury by a single intraperitoneal injection of folic acid (250 mg/kg body weight for the 14-day experiment; 300 mg/kg body weight in PBS for the 129-day experiment). In the 14-day experiment, we subcutaneously administered $1,25(OH)_2D_3$ (0.6 μg/kg body weight), DLAM-iPr (60 μg/kg body weight), or DLAM-4P (60 μg/kg body weight) on the day after folic acid injection; other mice received vehicle (propylene glycol). In the 129-day experiment, mice were administered vehicle (propylene glycol), DLAM-iPr (60 μg/kg body weight), or DLAM-4P (60 μg/kg body weight) via a subcutaneously implanted osmotic pump (Alzet 1004; Alzet Osmotic Pump) 3 days after folic acid injection. The pumps were replaced every month. Mice were analyzed at 129 days after folic acid injection. Serum calcium and creatinine levels were measured with Fuji Dry-Chem (Fujifilm) using CA-P III and CRE-P III slides, respectively.

*Histological analysis*. For analysis of collagen deposition, paraffin-embedded kidneys were sectioned at 4 μm, and Masson's trichrome stain was

performed by standard procedure at the Laboratory Animal Resource Center, University of Tsukuba. The amount of collagen deposition (blue area) was then digitally quantified using Image J software as described previously (65). For immunofluorescence, the paraffin-embedded kidney sections were deparaffinized, rehydrated, heat-inactivated using autoclave, permeabilized with NP-40, and incubated with primary antibody against FSP-1 (DAKO Japan) or α-SMA (Sigma-Aldrich). We used Alexa Fluor 594–conjugated secondary antibody (Invitrogen).

*Statistics*. All values described in the text and figures are expressed as mean ± SD. Significance of differences was determined by 2-tailed Student's *t* test. A *P* value less than 0.05 was considered significant.

*Study approval*. All animal experiments were performed in accordance with institutional guidelines of Laboratory Animal Resource Center, University of Tsukuba.

## Acknowledgments

This work was supported by Grant-in-Aid for JSPS Fellows (to I. Ito and T. Waku) and MEXT Targeted Proteins Research Program (to J. Yanagisawa).

Received for publication November 13, 2012, and accepted in revised form August 15, 2013.

Address correspondence to: Junn Yanagisawa, Graduate School of Life and Environmental Sciences/Life Science Center of Tsukuba Advanced Research Alliance, University of Tsukuba, Tsukuba Science City, Ibaraki 305-8577, Japan. Phone: 81.29.853.7323; Fax: 81.29.853.7322; E-mail: junny@agbi.tsukuba.ac.jp.

1. Sporn MB, Roberts AB. TGF-β: problems and prospects. *Cell Regul*. 1990;1(12):875–882.
2. Roberts AB, Sporn MB. Physiological actions and clinical applications of transforming growth factor-beta (TGF-β). *Growth Factors*. 1993;8(1):1–9.
3. Feng XH, Derynck R. Specificity and versatility in tgf-beta signaling through Smads. *Annu Rev Cell Dev Biol*. 2005;21:659–693.
4. Massague J, Seoane J, Wotton D. Smad transcription factors. *Genes Dev*. 2005;19(23):2783–2810.
5. Luo K, Lodish HF. Positive and negative regulation of type II TGF-β receptor signal transduction by autophosphorylation on multiple serine residues. *EMBO J*. 1997;16(8):1970–1981.
6. Wrana JL, Attisano L, Wieser R, Ventura F, Massague J. Mechanism of activation of the TGF-β receptor. *Nature*. 1994;370(6488):341–347.
7. Heldin CH, Miyazono K, ten Dijke P. TGF-β signalling from cell membrane to nucleus through SMAD proteins. *Nature*. 1997;390(6659):465–471.
8. Abdollah S, Macias-Silva M, Tsukazaki T, Hayashi H, Attisano L, Wrana JL. TβRI phosphorylation of Smad2 on Ser465 and Ser467 is required for Smad2-Smad4 complex formation and signaling. *J Biol Chem*. 1997;272(44):27678–27685.
9. Liu X, Sun Y, Constantinescu SN, Karam E, Weinberg RA, Lodish HF. Transforming growth factor β-induced phosphorylation of Smad3 is required for growth inhibition and transcriptional induction in epithelial cells. *Proc Natl Acad Sci U S A*. 1997; 94(20):10669–10674.
10. Eppert K, et al. MADR2 maps to 18q21 and encodes a TGFβ-regulated MAD-related protein that is functionally mutated in colorectal carcinoma. *Cell*. 1996;86(4):543–552.
11. Lagna G, Hata A, Hemmati-Brivanlou A, Massague J. Partnership between DPC4 and SMAD proteins in TGF-β signalling pathways. *Nature*. 1996; 383(6603):832–836.
12. Zhang Y, Feng X, We R, Derynck R. Receptor-associated Mad homologues synergize as effectors of the TGF-β response. *Nature*. 1996;383(6596):168–172.
13. Zhang YE. Non-Smad pathways in TGF-β signaling. *Cell Res*. 2009;19(1):128–139.
14. Noble NA, Border WA. Angiotensin II in renal fibrosis: should TGF-β rather than blood pressure be the therapeutic target? *Semin Nephrol*. 1997; 17(5):455–466.
15. Border WA, Okuda S, Languino LR, Sporn MB, Ruoslahti E. Suppression of experimental glomerulonephritis by antiserum against transforming growth factor β 1. *Nature*. 1990;346(6282):371–374.
16. Gaedeke J, Peters H, Noble NA, Border WA. Angiotensin II, TGF-β and renal fibrosis. *Contrib Nephrol*. 2001; (135):153–160.
17. Zeisberg M, Neilson EG. Mechanisms of tubulointerstitial fibrosis. *J Am Soc Nephrol*. 2010; 21(11):1819–1834.
18. Okuda S, Languino LR, Ruoslahti E, Border WA. Elevated expression of transforming growth factor-β and proteoglycan production in experimental glomerulonephritis. Possible role in expansion of the mesangial extracellular matrix. *J Clin Invest*. 1990;86(2):453–462.
19. Massague J. TGFβ in cancer. *Cell*. 2008; 134(2):215–230.
20. Eddy AA. Molecular insights into renal interstitial fibrosis. *J Am Soc Nephrol*. 1996;7(12):2495–2508.
21. Klahr S, Morrissey J. Obstructive nephropathy and renal fibrosis. *Am J Physiol Renal Physiol*. 2002;83(5):F861–F875.
22. Chevalier RL, Forbes MS, Thornhill BA. Ureteral obstruction as a model of renal interstitial fibrosis and obstructive nephropathy. *Kidney Int*. 2009; 5(11):1145–1152.
23. Klein J, et al. Renal fibrosis: insight from proteomics in animal models and human disease. *Proteomics*. 2011;1(8):805–815.
24. Flanders KC, et al. Mice lacking Smad3 are protected against cutaneous injury induced by ionizing radiation. *Am J Pathol*. 2002;60(3):1057–1068.
25. Schnabl B, Kweon YO, Frederick JP, Wang XF, Rippe RA, Brenner DA. The role of Smad3 in mediating mouse hepatic stellate cell activation. *Hepatology*. 2001;4(1):89–100.
26. Sato M, Muragaki Y, Saika S, Roberts AB, Ooshima A. Targeted disruption of TGF-β1/Smad3 signaling protects against renal tubulointerstitial fibrosis induced by unilateral ureteral obstruction. *J Clin Invest*. 2003;112(10):1486–1494.
27. Inazaki K, et al. Smad3 deficiency attenuates renal fibrosis, inflammation,and apoptosis after unilateral ureteral obstruction. *Kidney Int*. 2004;6(2):597–604.
28. Fujimoto M, et al. Mice lacking Smad3 are protected against streptozotocin-induced diabetic glomerulopathy. *Biochem Biophys Res Commun*. 2003; 05(4):1002–1007.
29. Zhao J, et al. Smad3 deficiency attenuates bleomycin-induced pulmonary fibrosis in mice. *Am J Physiol Lung Cell Mol Physiol*. 2002;82(3):L585–L593.
30. Chambon P. A decade of molecular biology of retinoic acid receptors. *FASEB J*. 1996;0(9):940–954.
31. Mangelsdorf DJ, et al. The nuclear receptor superfamily: the second decade. *Cell*. 1995;83(6):835–839.
32. McKenna NJ, O'Malley BW. Combinatorial control of gene expression by nuclear receptors and coregulators. *Cell*. 2002;108(4):465–474.
33. Tora L, et al. The human estrogen receptor has two independent nonacidic transcriptional activation functions. *Cell*. 1989;59(3):477–487.
34. Rochel N, Wurtz JM, Mitschler A, Klaholz B, Moras D. The crystal structure of the nuclear receptor for vitamin D bound to its natural ligand. *Mol Cell*. 2000; 5(1):173–179.
35. Heery DM, Kalkhoven E, Hoare S, Parker MG. A signature motif in transcriptional co-activators mediates binding to nuclear receptors. *Nature*. 1997; 387(6634):733–736.
36. Szpirer J, et al. The Sp1 transcription factor gene (SP1) and the 1,25-dihydroxyvitamin D3 receptor gene (VDR) are colocalized on human chromosome arm 12q and rat chromosome 7. *Genomics*. 1991; 11(1):168–173.
37. Palmer HG, et al. Vitamin D(3) promotes the differentiation of colon carcinoma cells by the induction of E-cadherin and the inhibition of β-catenin signaling. *J Cell Biol*. 2001;154(2):369–387.
38. Shah S, et al. The molecular basis of vitamin D receptor and β-catenin crossregulation. *Mol Cell*. 2006; 21(6):799–809.
39. Haussler MR, Jurutka PW, Mizwicki M, Norman AW. Vitamin D receptor (VDR)-mediated actions of 1α,25(OH)(2)vitamin D(3): genomic and nongenomic mechanisms. *Best Pract Res Clin Endocrinol Metab*. 2011;25(3):543–559.
40. Levi M. Nuclear receptors in renal disease. *Biochim Biophys Acta*. 2011;1812(8):1061–1067.
41. Li YC, Kong J, Wei M, Chen ZF, Liu SQ, Cao LP. 1,25-Dihydroxyvitamin D(3) is a negative endocrine regulator of the renin-angiotensin system. *J Clin Invest*. 2002;110(2):229–238.
42. Li Y, Spataro BC, Yang J, Dai C, Liu Y. 1,25-dihydroxyvitamin D inhibits renal interstitial myofibroblast activation by inducing hepatocyte growth factor expression. *Kidney Int*. 2005; 68(4):1500–1510.
43. Yuan W, et al. 1,25-dihydroxyvitamin D3 suppresses renin gene transcription by blocking the activity of the cyclic AMP response element in the renin gene promoter. *J Biol Chem*. 2007;282(41):29821–29830.
44. Zhang Z, et al. 1,25-Dihydroxyvitamin D3 targeting of NF-κB suppresses high glucose-induced MCP-1 expression in mesangial cells. *Kidney Int*. 2007;72(2):193–201.
45. Freundlich M, et al. Suppression of renin-angiotensin gene expression in the kidney by paricalcitol. *Kidney Int*. 2008;74(11):1394–1402.
46. Tan X, Wen X, Liu Y. Paricalcitol inhibits renal inflammation by promoting vitamin D receptor-mediated sequestration of NF-κB signaling. *J Am Soc Nephrol*. 2008;19(9):1741–1752.
47. Deb DK, et al. 1,25-Dihydroxyvitamin D3 suppresses high glucose-induced angiotensinogen expression in kidney cells by blocking the NF-κB pathway. *Am J Physiol Renal Physiol*. 2009; 296(5):F1212–F1218.
48. Zhang Y, Kong J, Deb DK, Chang A, Li YC. Vitamin D receptor attenuates renal fibrosis by suppressing the renin-angiotensin system. *J Am Soc Nephrol*. 2010; 21(6):966–973.
49. Tan X, Li Y, Liu Y. Paricalcitol attenuates renal interstitial fibrosis in obstructive nephropathy. *J Am Soc Nephrol*. 2006;17(12):3382–3393.
50. Samarakoon R, Overstreet JM, Higgins SP, Higgins P. J. TGF-β1 → SMAD/p53/USF2 → PAI-1 transcriptional axis in ureteral obstruction-induced renal fibrosis. *Cell Tissue Res*. 2011;347(1):117–128.

51. Dennler S, Itoh S, Vivien D, ten Dijke P, Huet S, Gauthier JM. Direct binding of Smad3 and Smad4 to critical TGF β-inducible elements in the promoter of human plasminogen activator inhibitor-type 1 gene. *EMBO J*. 1998;17(11):3091–3100.
52. Alroy I, Towers TL, Freedman LP. Transcriptional repression of the interleukin-2 gene by vitamin D3: direct inhibition of NFATp/AP-1 complex formation by a nuclear hormone receptor. *Mol Cell Biol*. 1995; 15(10):5789–5799.
53. Ishizuka S, Sato J, Takahama S, Seino Y, Norman AW. Serum concentrations of 1α,25(OH)2D3-26,26-lactone in normal adults. In: Norman AW, Bouillon R, Thomasset M, eds. *Vitamin D: Gene Regulation, Structure-Function Analysis and Clinical Application*. Berlin, Germany: Walter de Gruyter; 1991:300–301.
54. Nakano Y, et al. Practical synthesis and evaluation of the biological activities of 1α,25-dihydroxyvitamin D3 antagonists, 1α,25-dihydroxyvitamin D3-26,23-lactams. Designed on the basis of the helix 12-folding inhibition hypothesis. *J Med Chem*. 2006;49(8):2398–2406.
55. Robinson DM, Scott LJ. Paricalcitol: a review of its use in the management of secondary hyperparathyroidism. *Drugs*. 2005;65(4):559–576.
56. Bechtel W, et al. Methylation determines fibroblast activation and fibrogenesis in the kidney. *Nat Med*. 2010;16(5):544–550.
57. Ohnuma N, Bannai K, Yamaguchi H, Hashimoto Y, Norman AW. Isolation of a new metabolite of vitamin D produced in vivo, 1 α,25-dihydroxyvitamin D3-26,23-lactone. *Arch Biochem Biophys*. 1980; 204(1):387–391.
58. Ishizuka S, Norman AW. Metabolic pathways from 1 α,25-dihydroxyvitamin D3 to 1 α,25-dihydroxyvitamin D3-26,23-lactone. Stereo-retained and stereo-selective lactonization. *J Biol Chem*. 1987; 262(15):7165–7170.
59. Horst RL, Wovkulich PM, Baggiolini EG, Uskokovic MR, Engstrom GW, Napoli JL. (23S)-1,23,25-Trihydroxyvitamin D3: its biologic activity and role in 1 α,25-dihydroxyvitamin D3 26,23-lactone biosynthesis. *Biochemistry*. 1984;23(17):3973–3979.
60. Cianferotti L, Marcocci C. Subclinical vitamin D deficiency. *Best Pract Res Clin Endocrinol Metab*. 2012; 26(4):523–537.
61. Ding N, et al. A vitamin D receptor/SMAD genomic circuit gates hepatic fibrotic response. *Cell*. 2013; 153(3):601–613.
62. Ito I, et al. Estrogen inhibits transforming growth factor β signaling by promoting Smad2/3 degradation. *J Biol Chem*. 2010;285(19):14747–14755.
63. Zawel L, et al. Human Smad3 and Smad4 are sequence-specific transcription activators. *Mol Cell*. 1998;1(4):611–617.
64. Shi Y, Wang YF, Jayaraman L, Yang H, Massague J, Pavletich NP. Crystal structure of a Smad MH1 domain bound to DNA: insights on DNA binding in TGF-β signaling. *Cell*. 1998;94(5):585–594.
65. Zeisberg EM, Potenta SE, Sugimoto H, Zeisberg M, Kalluri R. Fibroblasts in kidney fibrosis emerge via endothelial-to-mesenchymal transition. *J Am Soc Nephrol*. 2008;19(12):2282–2287.